

Metasomatism in the Ultrahigh-pressure Svartberget Garnet-peridotite (Western Gneiss Region, Norway): Implications for the Transport of Crust-derived Fluids within the Mantle

J. C. VRIJMOED^{1*}, H. AUSTRHEIM², T. JOHN³, R. C. HIN⁴, F. CORFU⁵
AND G. R. DAVIES⁶

¹INSTITUTE OF EARTH SCIENCES, UNIVERSITY OF LAUSANNE, QUARTIER UNIL-MOULINE, BÂTIMENT GÉOPOLIS, CH-1015, LAUSANNE, SWITZERLAND

²PHYSICS OF GEOLOGICAL PROCESSES, UNIVERSITY OF OSLO, PO BOX 1048 BLINDERN, 0316, OSLO, NORWAY

³INSTITUT FÜR MINERALOGIE, UNIVERSITÄT MÜNSTER, CORRENSSTR. 24, 48149 MÜNSTER, GERMANY

⁴INSTITUTE FOR GEOCHEMISTRY AND PETROLOGY, ETH ZENTRUM, CLAUSIUSSTRASSE 25, 8092 ZÜRICH, SWITZERLAND

⁵GEOSCIENCE DEPARTMENT, UNIVERSITY OF OSLO, PO BOX 1047 BLINDERN, 0316, OSLO, NORWAY

⁶DEPARTMENT OF PETROLOGY, FACULTY OF EARTH AND LIFE SCIENCES, VRIJE UNIVERSITEIT, DE BOELELAAN 1085, 1081 HV, AMSTERDAM, NETHERLANDS

RECEIVED FEBRUARY 13, 2011; ACCEPTED MAY 7, 2013
ADVANCE ACCESS PUBLICATION JULY 1, 2013

Garnet-peridotites often contain veins or layers of pyroxenite and eclogite of uncertain origin. We investigate the Svartberget garnet-peridotite from the northernmost ultrahigh-pressure domain in the Western Gneiss Region (WGR) in Norway and show that the observed layering represents a sequence of metasomatic reaction zones developed along a fracture system. From the garnet-peridotite wall-rock to the fractures the following sequential reaction zones are recognized: clinohumite bearing garnet-peridotite, olivine-garnet-websterite, garnet-websterite, orthopyroxene-phlogopite-garnet-websterite, coarse-grained phlogopite-garnet-websterite, phlogopite-garnet-websterite, phlogopite-free garnet-websterite, inclusion-rich garnetite, garnetite, eclogite, retrograde omphacitite and felsic amphibole-pegmatite. The MgO, FeO and CaO contents generally decrease from the pristine peridotite towards the most metasomatized samples, with an associated increase in SiO₂ and Al₂O₃. Concentrations of fluid-mobile elements increase from the most pristine peridotite towards the garnetite, whereas Ni and Cr decrease from ~700 to ~10 ppm and ~2600 to ~25 ppm, respectively. Changes in mineral mode are accompanied by changes in mineral chemistry. All minerals

display decreasing Mg# and Cr content with degree of metasomatism, whereas Na₂O concentrations in amphibole, and most notably in clinopyroxene, increase from 0.2 to 3.0 and from 0.2 to 8 wt %, respectively. The trivalent ions Cr and Al display complex intra-granular vein-like or patchy zoning in garnet and pyroxenes that may be characteristic of metasomatized peridotites. Dating by the U–Pb method suggests metamorphic growth of zircon in the garnetite at 397.2 ± 1.2 Ma, formation of leucosomes in host-rock gneiss at 391.2 ± 0.8 Ma, and amphibole-pegmatite in the core of a garnetite vein at 390.1 ± 0.9 Ma. Initial ⁸⁷Sr/⁸⁶Sr values calculated at 397 Ma are elevated (~0.723) in the most pristine peridotites and increase to ~0.743 in the most metasomatized samples. The initial ⁸⁷Sr/⁸⁶Sr values of both the host gneiss and its leucosomes are also elevated (0.734–0.776), which suggests that the leucosomes found in the gneisses are the most likely, now solidified, remnants of the reactive agent that metasomatized the Svartberget peridotite. A scenario is envisaged in which material derived from the country rock gneiss was the source of the metasomatic addition of elements to the peridotites and the gneisses acted as the host for all elements removed

*Corresponding author: Telephone: 0041 21 692 43 10.
E-mail: johannes.vrijmoed@unil.ch

from the peridotite. The Svartberget peridotite may provide an important analogue of how felsic, slab-derived material interacts with the overlying mantle wedge peridotite in regions of arc magma generation.

KEY WORDS: garnet-peridotite; mantle wedge metasomatism; ultra-high-pressure metamorphism; metasomatic eclogite; Western Gneiss Region

INTRODUCTION

'Alpine-type' or 'orogenic' garnet-bearing peridotites, usually called garnet-peridotites, are mantle-derived rocks that are found within the crust in every major mountain range formed by continent–continent collision (Brueckner & Medaris, 2000; Bodinier & Godard, 2003). Orogenic peridotites are usually associated with eclogites; for example, Alpe Arami and Balmuccia in the European Alps, the Ronda massif in Spain, garnet-peridotites from the Western Gneiss Region (WGR) in Norway, the Moldanubian Zone of the Bohemian Massif, Czech Republic, and the Dabie Sulu ultrahigh-pressure (UHP) terrane, China (Carswell, 1990; Coleman & Wang, 1995). Garnet-peridotites in (U)HP terranes are often cut by veins or layers of pyroxenite and in some cases by eclogite (Brueckner & Medaris, 2000; Bodinier & Godard, 2003). The pyroxenites and eclogites are in many cases interpreted to be high-pressure crystal cumulates (Jamtveit, 1987; Bodinier *et al.*, 2008) from melts that invaded the peridotites while they were still in the mantle (Beard *et al.*, 1992; Medaris *et al.*, 1995; Becker, 1996). In other cases pyroxenites are interpreted as the result of metasomatism by melts of mantle or crustal origin (Sekine & Wyllie, 1982; Rampone & Morten, 2001; Malaspina *et al.*, 2006).

Based on mineral textures, mineral and whole-rock chemistry, and geochronology of garnet-bearing assemblages, garnet-peridotites are commonly divided into two types, one of mantle and the second of 'crustal' origin (Brueckner & Medaris, 2000). In this terminology, the crustal origin refers to the idea that most of these peridotites originated from mafic magmas that underwent magmatic differentiation in the crust to form lower crustal igneous intrusions (Brueckner & Medaris, 2000). The mantle and crustal type peridotites are often referred to as Mg–Cr type and Fe–Ti type garnet-peridotites, respectively (Carswell *et al.*, 1983). The garnet-bearing assemblages in Mg–Cr type garnet-peridotites originated from one or more high-pressure events in the mantle (Medaris *et al.*, 1995; Brueckner *et al.*, 2004; Spengler *et al.*, 2006) and were overprinted by (U)HP orogenic processes after or during incorporation into the crust (Medaris *et al.*, 1995; Scambelluri *et al.*, 2008). In contrast, the Fe–Ti type garnet-peridotites obtained their garnet assemblages by high-pressure orogenic processes overprinting the original

lower pressure (plagioclase or spinel) assemblages (Krogh & Carswell, 1995). In a review paper, Reverdatto *et al.* (2008) described geochemical criteria to distinguish these two genetically different types of peridotite, even after they have been subjected to a long geological history after their original emplacement. The criteria are based on distinctions between the contents of MgO, FeO, TiO₂, Cr, Ni, Zr, Nb and rare earth elements (REE) in peridotites and pyroxenites. [For further details, see Reverdatto *et al.* (2008).] Both Mg–Cr type peridotites and Fe–Ti type peridotites were identified by Carswell *et al.* (1983) in the WGR in Norway. The Svartberget peridotite has been classified as a crustal type (Fe–Ti type) peridotite based on its mineralogical characteristics (Vrijmoed *et al.*, 2006). However, following the classification of Reverdatto *et al.* (2008) based on bulk-rock chemistry, the Svartberget peridotite shows more affinity to Mg–Cr type peridotites (MgO ~27 wt %; Cr ~2600 ppm).

Irrespective of their complex origin, exhumed ultramafic bodies included in continental crustal sequences may provide the only accessible natural, large-scale, laboratories with which to investigate the mechanical and chemical effects of fluid and element transfer into the mantle wedge above subduction zones down to depths corresponding to UHP conditions. In this study we investigate in detail the Svartberget peridotite, which is cut by a network of pyroxenites, garnetites and eclogites. These veins represent metasomatic reaction zones formed when a reactive agent derived from the felsic Proterozoic host-rock gneiss of the WGR basement infiltrated through a conjugate set of fractures and interacted with the peridotite. Geothermobarometry studies of the garnet-peridotite and the crosscutting websterite veins indicate peak-metamorphic conditions of about 800°C at ~5.5 GPa (Vrijmoed *et al.* 2006). Accordingly, the Svartberget peridotite provides a well-exposed example of 'frozen-in' mantle–crust interaction.

Geochronology studies demonstrate that part of the migmatization of the host-rock gneisses might have occurred during a UHP event within the WGR; we propose that the resulting fluids formed the infiltrating reactive agent that modified the peridotites. Textural and Sr isotope data indicate that even the most pristine peridotite has undergone metasomatism, which may explain why the Svartberget peridotite exhibits characteristics of both crustal- and mantle-type peridotites.

THE SVARTBERGET PERIDOTITE

The Svartberget peridotite is located in the WGR in Norway, which formed part of the crust of Baltica prior to the formation of the Caledonian orogenic belt. Textures, mineral assemblages and structures within the WGR became modified as a result of the collision of Baltica with the continent Laurentia, which started at ~425 Ma

(e.g. Mørk, 1985; Torsvik *et al.*, 1996; Andersen, 1998). During this collision the WGR was subjected to (U)HP metamorphic conditions at relatively low temperatures, conditions now recorded by the eclogites and peridotites (Carswell & Cuthbert, 2003).

The Svartberget peridotite body, first described by Vrijmoed *et al.* (2006), is located within Proterozoic crustal gneiss of the WGR that records evidence for multiple melting events, resulting in several generations of leucosomes (Labrousse *et al.*, 2011). The peridotite body is crosscut by a network of oriented fractures consisting of phlogopite–garnet–websterite veins. Vrijmoed *et al.* (2006) reported highly radiogenic initial Sr isotope ratios (corrected to Caledonian ages) in clinopyroxene from a diamond-bearing phlogopite–garnet–websterite vein. These isotopic data suggest metasomatism of the peridotite and a crustal origin for the veins. The veins record the highest initial Sr isotope ratios, suggesting that they were the main fluid channels during infiltration of transitional fluids (Hermann *et al.*, 2006) from the gneiss into the peridotite.

Geothermobarometry studies of garnet–peridotite samples and crosscutting websterite veins (Vrijmoed *et al.*, 2006) have indicated that the garnet–clinopyroxene thermometer of Powell (1985) in combination with the Al-in-orthopyroxene barometer of Brey & Köhler (1990) are the most applicable to determine peak metamorphic conditions for the websterite veins; these yielded conditions of 5.5 GPa at 800°C. Garnet in the websterite veins has polyphase solid inclusion assemblages including microdiamond (Vrijmoed *et al.*, 2008). At these *P–T* conditions these polyphase inclusions most probably precipitated from a transitional fluid [following the definition in Hermann *et al.* (2006)] and indicate that vein formation occurred under UHP conditions. The garnet–olivine thermometer of O'Neill & Wood (1979), using the correction of O'Neill (1980), in combination with the Al-in-orthopyroxene barometer of Brey & Köhler (1990) are considered the most applicable for the garnet–peridotites and yielded pressures of 3.4 GPa at 800°C.

SAMPLE DESCRIPTION

To obtain a better understanding of the relationships between garnetites, websterites, and the host peridotite, the body was mapped in great detail and the size of the different blocks, structures, and lithological units measured. The mapping was performed at a scale of 1:25 using georeferenced orthogonally projected aerial photographs (orthophotos) from Statens Kartverk and 1:5000 topographic (Økonomisk Kartverk) maps. The resultant map was digitized using ArcGIS mapping software. A simplified version of the map is shown in Fig. 1. (The full map is available online as Supplementary Data, Suppl. Fig. 1, available for downloading at <http://www.petrology.oxfordjournals.org>).

The key field observations, summarized in Figs 2 and 3, show a transition from the core of the peridotite and olivine–websterite wall-rocks to websterite, followed by garnetite and locally to eclogite, that ultimately ends in a pegmatitic felsic rock in the middle of the veins. The entire lithological sequence is not found in any single section from the wall-rock across the veins (see Suppl. Fig. 2 for schematic overview of the possible sequences of lithological zones). The characteristic mineralogy, structures and textures of the zones are described below in three main groups: (1) wall-rocks (peridotite and olivine–websterite); (2) transition from wall-rocks to veins (pyroxenite); (3) primary veins (pyroxenite or garnetite) (Table 1; Figs 2 and 3). Two sets of dominant veins can be observed in the Svartberget body. The primary veins are the oldest set of veins that appear to have formed along a conjugate set of fractures (Vrijmoed *et al.*, 2009). Secondary veins formed along a set of subparallel, subvertical fractures that crosscut the primary veins. The focus of this study is on the mineralogical zonations in the primary veins and associated wall-rocks. A brief description is given below of some primary veins that did not fully develop (immature veins), the secondary veins and the host gneiss. Mineral modes were estimated from point counting, and by least-squares optimization using bulk-rock chemistry (Table 2 and Suppl. Data Tables 2–6) combined with mineral chemistry (Table 3).

Wall-rocks

This group of rock types are found as peridotite and websterite blocks (Fig. 2a and b) that form the wall-rock of the crosscutting veins. Generally the smaller the blocks, the more pyroxenitic they become. Zones 1–3 represent, respectively, the most and the least olivine and Fe–Ti oxide bearing rock types.

Zone 1 (olivine-bearing rocks)

Rocks of zone 1 are all olivine-bearing and can be divided into two main groups: peridotite (zone 1a and b) and olivine–websterite (zone 1c). Peridotites from zone 1a and b are found only in the northern part and olivine–websterites from zone 1c are found only in the southern part of the study area.

Zone 1a: spinel–garnet–peridotites, gp. Spinel–garnet–peridotite consists of roughly 30% olivine of which 12–15% is altered to a late-stage yellow serpentine-like mineral, 25% clinopyroxene, 20% orthopyroxene, 15% garnet, 5% Fe–Ti oxides and about 5% kelyphite and <1% amphibole (Table 1). In hand specimen the rock is homogeneous equigranular with pale olive green to brownish colours. In a few (<10) localities in the northeastern part of the body the blocks are slightly foliated. The texture of the peridotite is characterized by a network defined by olivine with minor orthopyroxene, clinopyroxene, garnet and oxides (Fig. 4a and b; for back-scattered electron image see Suppl. Data Fig. 3a and b). This network encloses poikilitic

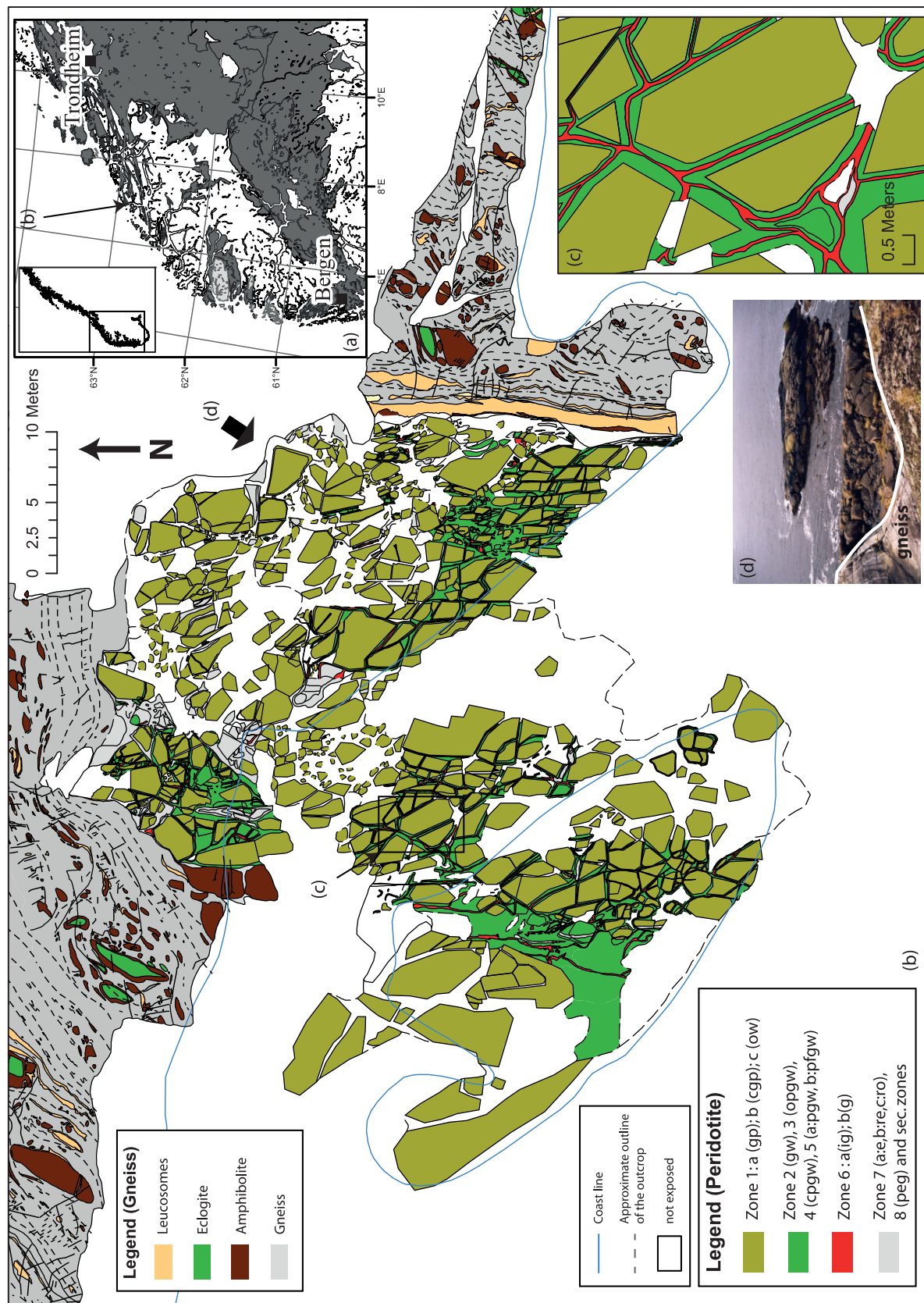


Fig. 1. Geological map of the Svartberget peridotite body and host gneiss. (a) Simplified tectonic map of the WGR. Caledonian nappes and basement cover are indicated in dark gray, Devonian basins in light gray and WGR in white. Location of Svartberget indicated by the arrow. Inset shows geographical location of the regional map. (b) A simplified map of the Svartberget peridotite body and surrounding gneiss (for a more detailed map see Supplementary Data Fig. 1) shows how the body is cut by numerous fractures forming a conjugate set along which metamorphic zones developed. (c) A close-up of part of (b) illustrates the symmetric arrangement of metamorphic reaction zones. (d) Field photograph view of the Svartberget body. Viewpoint indicated with wide arrow in (b).

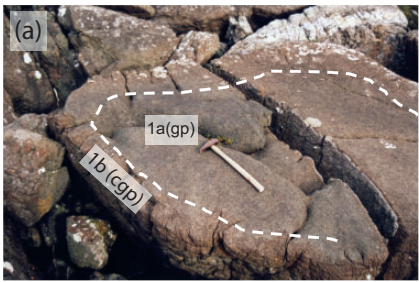
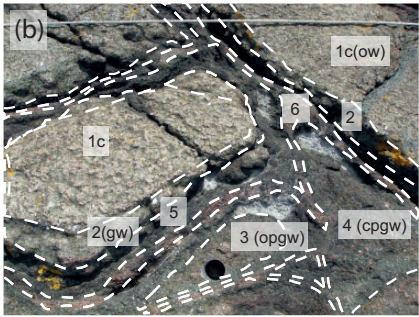
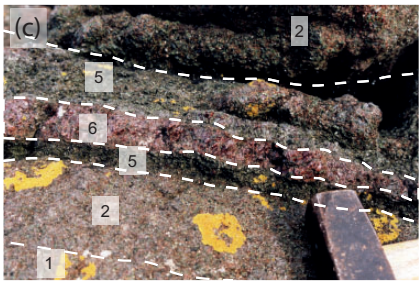
Field	Mineralogy	Min-chemistry	Z	Lithology	Outcrop
(a) 	30 % Ol 25 % Cpx 20% Opx 15 % Grt 5 % { Mt Ilm Sp	Fo ₈₄ En ₄₉ Fs ₂ Wo ₄₉ Jd _{1.4} En ₈₆ Fs ₁₄ Py ₅₇ Alm ₂₇ Gr ₁₄ Spss ₂ Mt ₈₀ Cr ₁₄ Sp ₆	1a 1b	Peridotite ↓	
(b) 	6-15% Ol 42% Cpx 20-30% Opx 20% Grt 3% Mt-Ilm-Sp		1c 2 & 3	Pyroxenite ↓	Wall rocks
(c) 	35-55% Cpx 20% Opx 15% Grt 10% Phl 1-20% Amph	En ₄₆ Fs ₈ Wo ₄₆ Jd ₄ En ₈₂ Fs ₁₈ Py ₅₀ Alm ₃₅ Gr ₁₃ Spss ₂ Phl ₈₅ tschermakite	4 & 5	↓	Transition
	98-100% Grt 0-2% { Phl (Opx) (Cpx)	Py ₅₆ Alm ₂₉ Gr ₁₃ Spss ₂ Phl ₈₃ En ₇₈ Fs ₂₂ En ₄₉ Fs ₂ Wo ₄₉ Jd ₂	6	Garnetite	Primary veins

Fig. 2. Field relations. Field photographs (a)–(c) document the stages of metasomatism of the peridotite and the appearance of the metasomatic zones in outcrop. The second column shows the changes in the mineral assemblages and the associated change in mineral chemistry from the peridotite (zone 1a) towards the fracture-filling garnetite (zone 6). An indication of the mineral mode is given in volume percentage, based on the general field appearance combined with thin-section point counting. The zones (Z) are numbered in the third column. The rock type abbreviations are those used throughout the text: gp, garnet-peridotite; cgp, clinohumite-bearing garnet-peridotite; ow, olivine-websterite; gw, garnet-websterite; opgw, orthopyroxene-phlogopite-garnet-websterite; cpgw, coarse-grained phlogopite-garnet-websterite. The appearance of the rock type in outcrop, as wall-rock or veins is indicated in the last column. Ol, olivine; Cpx, clinopyroxene; Opx, orthopyroxene; Grt, garnet; Mt, magnetite; Ilm, ilmenite; Sp, spinel; Phl, phlogopite; Amph, amphibole.

patches dominated by garnet with ortho- and clinopyroxene, and grains of Fe–Ti oxides (Fig. 5a–c). Garnets are generally medium grained and 1–5 mm in diameter, but smaller grains also occur (<1 mm). When in contact, clinopyroxene and orthopyroxene generally display equilibrium textures, but are in many cases resorbed by garnet (Fig. 5d; for back-scattered electron image see Suppl. Data Fig. 4). Clinopyroxene typically has areas rich in inclusions of fine-grained (<10 µm) Cr-bearing spinel (Fig. 5a, in lower left corner, and Fig. 5c). Such areas constitute ~50% of the clinopyroxene. Occasionally, clinopyroxene in contact with orthopyroxene has resorbed grain boundaries suggesting that orthopyroxene replaced clinopyroxene. Larger magnetite–ilmenite and spinel (~25–100 µm) grains are found as inclusions, as well as interstitially in

triple junctions in olivine-dominated networks, and to a lesser extent in garnet–clinopyroxene–orthopyroxene patches, and occur as aggregates that usually consist of about one-third green pleonaste spinel and two-thirds opaque oxides (Fig. 5a and c). Symplectite intergrowths (kelyphite), consisting of spinel, orthopyroxene and clinopyroxene, often occur between garnet and olivine (Fig. 5).

Zone 1b: clinohumite garnet-peridotite zone, cgp. In at least eight localities of the ~710 mapped blocks of the Svartberget body, the garnet-peridotite blocks of zone 1a show a 5–10 cm wide rim characterized by cracks perpendicular to the veins (Fig. 2a). This zone contains fluorine-rich Ti-clinohumite (<1%) in addition to the mineral assemblage of zone 1a (Fig. 4c, Suppl. Data Fig. 3c). The clinohumite is surrounded by secondary olivine, which generally has

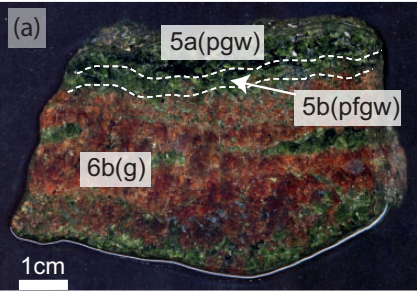
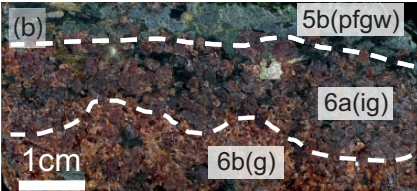
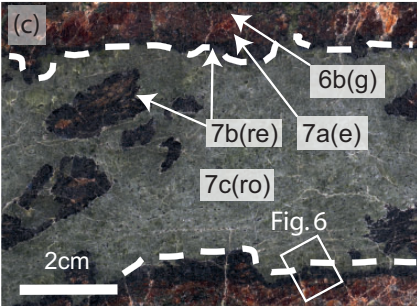
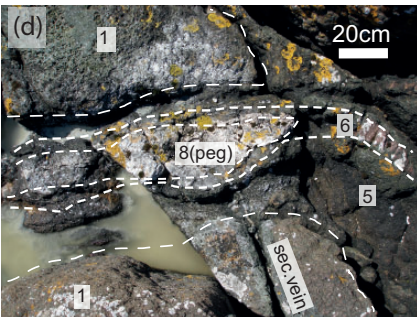
Field	Mineralogy	Min-chemistry	Z	Lithology	Outcrop
(a) 	30-55% Cpx 20% Opx 15% Grt 10% Phl 1-20% Amph	En ₄₆ Fs ₈ Wo ₄₆ Jd ₄ En ₈₂ Fs ₁₈ Py ₅₀ Alm ₃₅ Gr ₁₃ Spss ₂ Phl ₈₅ tschermakite	5a	Pyroxenite	
(b) 	80% Cpx 10% Opx 10% Grt		5b		
(c) 	98-100% Grt 0-2% { Phl (Opx) (Cpx)	Py ₅₆ Alm ₂₉ Gr ₁₃ Spss ₂ Phl ₈₃ En ₇₈ Fs ₂₂ En ₄₉ Fs ₂ Wo ₄₉ Jd ₂	6 & 7a	Garnetite	Primary veins
(d) 	50% Amph 50% Pl		7b	(Retro)-Eclogite	
	20% Omp 30% Amph 50% Pl	En ₄₆ Fs ₈ Wo ₄₆ Jd ₁₅ Ac ₁₁ Taramite Ab ₉₃ An ₇	7c	Retro - Omphacitite	
	30% Cpx+Amph 70% Pl+Qtz		8	Pegmatite core	

Fig. 3. Field relations. Field photographs (a)–(d) show the details of the garnetite–websterite veins and their transition to amphibole–pegmatite. The other columns are as in Fig. 2. Abbreviations: pgw, phlogopite–garnet–websterite; pfgw, phlogopite-free garnet–websterite; ig, inclusion-rich garnetite; g, garnetite; e, eclogite; re, retrogressed eclogite; ro, retrogressed omphacitite; peg, amphibole pegmatite; sec. vein, secondary vein; Omp, omphacite; Pl, plagioclase.

grown epitaxially on the neighbouring olivine. These secondary rims contain many submicron ilmenite grains, which are a product of the breakdown of Ti-clinohumite. The Ti in the clinohumite either has been introduced into the rock or comes from the breakdown of a Ti-bearing phase such as ilmenite.

Zone 1c: olivine-websterite, ow. The large blocks (15–20 m²) in the southwestern part of the body consist of garnet–olivine–websterite. They contain 6–15% olivine, 40% clinopyroxene, 20–30% orthopyroxene, 20% garnet, 3%

oxides and some amphibole (1%), phlogopite (<1%) and symplectite (<1%) (Table 1). The rock and minerals generally have the same features as previously described for the spinel–garnet–peridotite (zone 1a, Fig. 4d, Suppl. Data Fig. 3d), except for the lack of any foliation and that the rocks are less serpentinized.

Zone 2 (garnet-websterites, gw)

Wall-rock peridotite (zone 1a and b) and olivine–websterite (zone 1c) are rimmed with a 10–30 cm wide zone of

Table 1: Summary of the petrography of the Svartberget body

Sample	W.no.	Z	Loc	Size	Rock	OI	Cpx	Opx	Grt	FTox	Sp	Kely	Phl	Amph	C/S	Chu	Pl
SV03-07	23	1a	NE	3-48	gp	x	x	x	x	x	x	x	—	<1	x	—	—
SV03-8	87	1a	NE	0-77	gp	x	x	x	x	x	x	x	—	<1	x	—	—
SV04-2	14	1a	NE	10-4	gp	17-7	25-5	17-3	14-3	6-7	<1	2-9	—	0-2	15-5	—	—
SV05-1	36	1a	NE	3-66	gp	20-1	23-6	22-1	16-4	2-6	0-2	2-6	—	0	12-3	—	—
SV05-1A	36	1a	NE	3-66	gp	x	x	x	x	x	x	x	—	<1	x	—	—
SV05-1B	36	1a	NE	3-66	gp	x	x	x	x	x	x	x	—	<1	x	—	—
SV05-4	36	1a	NE	3-66	gp	x	x	x	x	x	x	x	—	<1	x	—	—
SV06-8	4	1a	NE	3-50	gp	x	x	x	x	x	x	x	—	<1	x	—	—
SV06-10	4	1a	NE	3-50	gp	x	x	x	x	x	x	x	—	<1	x	—	—
SV06-15	100	1a	NE	4-03	gp	x	x	x	x	x	x	x	—	<1	x	—	—
Total		1a	NE	671	gp	28-1	37-9	15-4	17-4	2-7	—	—	—	—	—	—	—
SV05-3	219	1b	NE	2-71	cgp	x	x	x	x	x	x	x	—	<1	x	<1	—
SV05-05A	36	1b	NE	3-66	cgp	x	x	x	x	x	x	x	—	<1	x	<1	—
SV05-05B	36	1b	NE	3-66	cgp	x	x	x	x	x	x	x	—	<1	x	<1	—
Total		1b	NE	7-17	cgp	27-5	38-9	18-9	11-5	3-5	0-9	—	—	—	—	—	—
SV04-31	112	1c	SW	17-4	ow	x	x	x	x	<1	—	<1	—	<1	<1	—	—
SV06-P1	112	1c	SW	17-4	ow	5-9	40-5	30	19-4	2-2	0-2	0-4	0-2	1-2	<1	—	—
SV06-P2	72	1c	SW	15-5	ow	x	x	x	x	<1	—	<1	—	<1	<1	—	—
SV06-17	72	1c	SW	15-5	ow	x	x	x	x	<1	—	<1	—	<1	<1	—	—
SV06-18	72	1c	SW	15-5	ow	x	x	x	x	<1	—	<1	—	<1	<1	—	—
SV06-19	72	1c	SW	15-5	ow	x	x	x	x	<1	—	<1	—	<1	<1	—	—
SV06-20	72	1c	SW	15-5	ow	x	x	x	x	<1	—	<1	—	<1	<1	—	—
SV06-21	72	1c	SW	15-5	ow	x	x	x	x	<1	—	<1	—	<1	<1	—	—
Total		1c	SW	*	ow	15-1	41-5	20-8	21	2-9	—	—	—	—	—	—	—
SV04-33	252	2	SE	3-80	gw	—	x	x	x	—	—	—	<1	<1	—	—	—
SV06-2	92	2	SW	0-06	gw	—	x	x	x	—	—	—	<1	<1	—	—	—
SV06-3	57	2	SW	1-75	gw	—	x	x	x	—	—	—	<1	<1	—	—	—
SV06-4	57	2	SW	1-75	gw	—	x	x	x	—	—	—	<1	<1	—	—	—
SV06-5	59	2	SW	0-17	gw	—	25-5	59-9	7-1	—	—	—	2-9	4-1	—	—	—
SV06-P3	57	2	SW	1-75	gw	—	x	x	x	—	—	—	<1	<1	—	—	—
Total†		2	SW	16-5	gw	—	30-8	42-9	26-9	—	—	—	—	—	—	—	—
SV06-6	253	3	SW	0-03	opgw	—	15-3	50-2	2-4	—	—	—	28-4	3-7	—	—	—
Total†		3	SW	0-44	opgw	—	42-2	37-9	0	—	—	—	22	—	—	—	—
SV04-32B	112, 51	4	SW		cpgw	—	9-8	48-5	27-6	—	—	—	3-3	10-7	—	—	—
SV06-P6	112, 50	4	SW		cpgw	—	x	x	x	—	—	—	x	x	—	—	—
SV06-P7	112, 57	4	SW		cpgw	—	34-2	19-1	2	—	—	—	8-4	35-3	—	—	—
Total		4	SW	153	cpgw	—	27-5	37-5	8	—	—	—	3-7	24-9	—	—	—
SV04-38A	254, 255	5a	NE		pgw	—	x	x	x	—	—	—	x	<1	—	—	—
Total		5a	NE	‡	pgw	—	64-5	5-4	20-3	—	—	—	9-5	0	—	—	—
SV04-38B	254, 255	5b	NE		pfgw	—	x	x	x	—	—	—		<1	—	—	—
Total†		5b	NE	‡	pfgw	—	82-3	1-1	17-5	—	—	—	—	—	—	—	—
SV06-1B	112, 57	6a	SW		ig	—	x	x	x	—	—	—	x	<1	—	—	—
Total†		6a	SW	31-7	ig	—	8-4	2-9	88-1	—	—	—	0-7	—	—	—	—
SV06-29B	162, 160	6b	NE		g	—	x	x	x	—	—	—	x	<1	—	—	—
SV06-P8	112, 50	6b	SW		g	—	x	x	x	—	—	—	x	<1	—	—	—
SV06-1A	112, 57	6b	SW		g	—	x	x	x	—	—	—	x	<1	—	—	—

(continued)

Table 1: Continued

Sample	W.no.	Z	Loc	Size	Rock	OI	Cpx	Opx	Grt	FTox	Sp	Kely	Phl	Amph	C/S	Chu	Pl
SV04-38	254, 255	6b	NE		g	—	x	x	x	—	—	—	x	<1	—	—	—
SV04-38C	254, 255	6b	NE		g	—	x	x	x	—	—	—	x	<1	—	—	—
SV06-22A	239, 256	6b	S		g	—	x	x	x	—	—	—	x	<1	—	—	—
<i>Total</i>		6b		§	g	—	8.4	2.9	88.1	—	—	—	0.7	—	—	—	—
SV06-22C	239, 256	7b	S		re	—	x	—	—	—	—	—	—	x	—	—	x
<i>Total</i>		7b	S	¶	re												
SV06-D1	224, 257	7c	S		ro	—	x	—	—	—	—	—	—	x	—	—	x
SV06-22B	239, 256	7c	S		ro	—	x	—	—	—	—	—	—	x	—	—	x
<i>Total</i>				3.18	ro	—	28.2	—	—	—	—	—	—	25.6	—	—	46.5
SV07-1	217, 258	8	S		peg	—	x	—	—	—	—	—	—	x	—	—	x
<i>Total</i>		8	S	0.39													
Perimeter	247																
Total secondary	36.0																
Total outcrop	833																
Total not exposed	591																
Total	1460																

W.no, wall-rock no.; Z, zone; Loc, location, Size in m², Rock, rock type; C/S, clay/serp; FTox, Fe-Ti oxide; Kely, kelyphite; gp, garnet-peridotite; cgp, clinohumite-bearing garnet-peridotite; ow, olivine-websterite; gw, garnet-websterite; opgw, coarse-grained orthopyroxene-rich phlogopite-garnet-websterite; cpgw, coarse-grained phlogopite-garnet-websterite; pgw, phlogopite-garnet-websterite; pfgw, phlogopite-free garnet-websterite; ig, inclusion-rich garnetite; g, garnetite; re, retrograde eclogite; ro, retrograde omphacite; peg, amphibolite pegmatite; x, mineral present; —, mineral absent. Secondary, secondary veins. Modes listed under 'Total' are calculated mineral modes. Other modes are obtained from point counting. Global positioning system coordinates of the samples can be found in Suppl. Table 10.

*Included in zone 1a.

†EMP analyses for mode calculation taken from a similar, but different, zone owing to a lack of mineral-chemical analyses for this zone.

‡Not estimated from map (see Fig. 3a).

§Not estimated from map (see Fig. 3b).

¶Not estimated from map (see Fig. 3c).

garnet-websterite that define zone 2. In addition, wall-rock blocks of intermediate size or smaller (<0.5 m²) are classified as zone 2 garnet-websterites (Fig. 2b). The samples are unfoliated, lack olivine and oxides, and are dominated by clinopyroxene and orthopyroxene (40–60% orthopyroxene, 25–30% clinopyroxene, 7–27% garnet, 4% amphibole, 3% phlogopite). Poikilitic garnets have more and smaller inclusions (0.4 vol. % and 1–10 µm) than in the other block groups. Crystals of clinopyroxene and orthopyroxene are more elongated (length/width ~3). Clusters of oxide inclusions are absent (Fig. 4e, Suppl. Data Fig. 3e). The classification of these samples into a single zone is arbitrary, as the transition to the zone 3 rock type is gradual.

Zone 3 (opx-rich phlogopite-garnet-websterites, opgw)

Blocks with a diameter less than 0.5 m are completely transformed into coarse-grained orthopyroxene-rich phlogopite-garnet-websterite (Fig. 2b). The rocks consist of ~50% orthopyroxene, 15% clinopyroxene, 30%

phlogopite and 5% garnet, with minor amphibole and rutile. The rock is homogeneous on the outcrop scale. However, phlogopite tends to occur as homogeneously distributed clusters. The overall colour is light brown owing to the abundance of orthopyroxene (Fig. 2b). The texture is coarse grained (1–7 cm) equigranular, and is made up of randomly oriented, elongated, euhedral clinopyroxene and orthopyroxene grains with phlogopite clusters. Owing to the phlogopite clusters and the large grain size, the sample is not homogeneous on the thin-section scale. Garnet is interstitial and anhedral, poikilitic, medium to coarse grained. Amphibole occurs as replacement rims around clinopyroxene. Rutile is fine grained, anhedral and occurs as inclusions.

Wall-rock to vein transition

One of the zones (zone 4) does not have a regular width like the primary veins, but the mineralogy is nearly identical to that of the adjacent zone (zone 5). Although it does

Table 2: Representative whole-rock analyses of the metasomatic zones in the Svartberget body

Zone:	1a,b	1c	2	3	4	5a	5b	6a	6b	7a	7b	7c	8	Leuco.	Gneiss
Rock:	gp	ow	gw	opgw	cgpw	pgw	pfgw	ig	g	e	re	ro	peg	leu	gn
Sample:	SV06	SV06	SV06	SV06	SV06	SV04	SV04	SV06	SV04	SV06	SV06	SV06	SV07	SV06	SV06
	8	P1	5	6	P6	38A	38B	1B	38C	22A	22C	22B	1	G1	
<i>Major elements (wt %)</i>															
SiO ₂	47.7	48.8	52.4	52.0	53.5	50.7	52.9	42.4	43.6	43.6	43.6	56.5	61.9	75.1	70.0
TiO ₂	0.15	0.20	0.19	0.25	0.19	0.48	0.16	1.09	0.22	0.34	0.12	0.12	0.04	0.03	0.57
Al ₂ O ₃	4.25	5.13	5.25	5.18	5.01	6.74	4.93	19.43	18.5	18.4	19.5	15.0	14.9	16.1	15.2
FeO _t	10.3	8.95	9.65	7.78	7.59	7.10	6.16	16.9	13.8	14.0	13.8	4.27	2.70	0.66	3.61
MnO	0.24	0.24	0.22	0.16	0.28	0.21	0.24	0.87	0.70	0.52	0.41	0.05	0.10	0.01	0.09
MgO	26.7	23.7	23.0	22.6	20.8	16.2	15.8	14.0	14.3	11.7	9.7	7.13	4.19	0.16	1.69
CaO	10.9	11.5	8.49	9.41	9.62	14.8	18.9	3.47	7.63	9.51	8.20	10.9	7.82	1.19	0.80
Na ₂ O	0.22	0.20	0.55	0.72	1.44	0.60	0.49	0.22	0.12	1.48	3.61	5.93	5.00	3.71	1.76
K ₂ O	0.01	0.02	0.25	2.15	0.96	1.29	0.07	1.09	0.02	0.03	0.04	0.03	0.32	2.56	3.97
P ₂ O ₅	0.01	0.02	0.16	<0.01	<0.01	<0.01	<0.01	0.01	0.05	0.72	0.15	0.01	0.30	0.05	0.03
Total	100	98.8	100	100	99.4	98.1	99.7	99.5	98.9	100	99.1	100	97.3	99.6	97.7
LOI	0.45	2.16	0.15	0.96	0.27	2.35	0.67	0.27	-0.01	0.24	0.82	0.45	n.d.	0.50	0.72
<i>Trace elements (ppm)</i>															
Rb	0.5	1.85	16.6	137	64	105	5.5	72	1.68	0.7	1.90	0.6	10.0	53	147
Ba	13.3	19.5	39	219	120	121	22.4	100	17.7	9.3	16.4	7.8	48	62	837
Sr	43.4	48.1	63.1	69.6	73.4	94.2	97.4	9.25	23.8	62.1	29.9	42.7	371	89.4	122
Pb	5.70	4.82	6.62	8.50	7.55	15.0	12.4	5.08	5.92	5.34	5.03	3.76	n.d.	13.3	14.0
Y	4.61	6.79	6.67	4.73	15.4	14.1	17.3	35.0	67.6	81.3	69.0	4.38	n.d.	5.26	13.1
Sc	40	n.d.	44	28	n.d.	47	40	37	45	31	15.3	10.5	n.d.	n.d.	n.d.
Zr	11.8	14.6	26.7	23.2	41.7	11.3	12.2	241	105	47.6	48.3	16.8	44	6.98	254
Nb	0.7	1.0	1.56	5.74	3.52	11.6	3.72	23.3	6.38	30.0	5.03	0.4	n.d.	3.62	13.4
Ga	4.69	n.d.	5.04	9.66	n.d.	7.86	4.47	11.1	6.02	9.9	9.35	20.0	n.d.	n.d.	n.d.
Zn	70.9	n.d.	82.8	88.4	n.d.	41.0	32.4	70.1	31.7	60.1	69.4	46.0	21.0	n.d.	n.d.
V	109	n.d.	93.7	117	n.d.	149	101	69.1	86.9	68.2	33.8	51.8	7.00	n.d.	n.d.
Cr	2430	2150	2150	1810	2030	2310	1310	1030	830	580	150	27	22	5.1	37
Cu	29.6	n.d.	10.9	14.5	n.d.	14.6	8.99	14.4	9.53	57.1	58.3	3.11	n.d.	n.d.	n.d.

leuc, leucosome; gn, gneiss; n.d., not determined; LOI, loss on ignition. (For rock abbreviations see Table 1.)

not form blocks that stand out in relief, locally it preserves the shapes of blocks. These rock types occur between the blocks and primary veins and therefore mark the transition from block to vein.

Zone 4 (coarse-grained phlogopite–garnet–websterite, cpgw)

The cores of the blocks described above are surrounded in three locations by undeformed coarse-grained to pegmatitic (5 mm to 40 cm) phlogopite–garnet–websterite (Fig. 2b). The zones vary in width from several decimetres to 2–3 m. On a metre scale the rock is homogeneous, but in thin section it is heterogeneous, both in terms of grain size and mineral assemblage, but has no foliation. Estimates of modal abundances in this rock type vary considerably between thin sections: 10–34% clinopyroxene,

20–50% orthopyroxene, 3–8% phlogopite, 2–28% garnet, 10–35% amphibole. Micrometre-sized monazite and sub-millimetre-sized rutile grains are present as anhedral inclusions in all minerals. Clinopyroxene and orthopyroxene are intergrown in clusters with phlogopite and garnet fills the intervening space. In thin section, clinopyroxene and orthopyroxene appear as elongated crystals with subhedral and euhedral crystal faces. Clinopyroxene crystals are often replaced by amphibole along grain boundaries that form embayment structures (Fig. 4f, Suppl. Data Fig. 3f). Phlogopite occurs as subhedral medium to coarse grains commonly interstitial between the orthopyroxene and clinopyroxene grains, with irregularly shaped edges and locally apparently resorbed by clinopyroxene and orthopyroxene. Garnet occurs as anhedral medium- to

Table 3: Average electron microprobe (EMP) measurements and endmember proportions from wall-rock garnet-peridotite (zone 1a and b, gp), phlogopite-garnet-websterite (zones 4 and 5), garnetite (zone 6), eclogite (zone 7a) and retro-omphacitite (zone 7c) in metasomatic veins in the Starberget peridotite body

Mineral:	4 and 5 (Coarse-grained Phl-Grt-websterite (cpgw, pgw, gw))									
	1a and b Garnet-peridotite (gp, cgp)		4		5		7		25	
	Cpx	Grt	Opx	Ol	Mt	Cpx	Grt	Opx	Phl	Amph
Grains (n):	9	12	9	4	5	5	11	7	1	4
Analyses (n):	91	134	51	31	5	117	142	109	25	5
<i>Oxides (wt %)</i>										
SiO ₂	54.4	0.63	0.54	0.28	0.31	0.03	0.52	0.49	0.24	0.35
TiO ₂	0.03	0.02	0.01	0.01	<0.01	2.90	0.01	<0.01	<0.01	0.02
Al ₂ O ₃	0.78	0.19	0.20	0.59	0.01	2.41	0.32	0.20	0.18	0.08
Cr ₂ O ₃	0.11	0.04	0.21	0.02	0.01	8.98	0.19	0.03	0.01	0.04
FeO	3.04	0.12	0.01	0.43	0.36	76.4	0.27	0.45	0.18	0.75
MgO	17.3	0.11	0.81	0.49	0.26	2.03	0.48	0.36	0.29	7.62
MnO	0.10	0.02	0.31	0.02	0.04	0.25	0.02	0.09	0.01	0.14
NiO	0.03	0.03	0.01	0.01	0.05	0.26	<0.01	n.d.	n.d.	0.25
CaO	24.2	0.26	0.19	0.03	0.01	0.23	0.85	0.20	0.01	0.79
Na ₂ O	0.39	0.12	0.01	0.02	0.01	0.01	0.23	0.01	<0.01	0.04
K ₂ O	<0.01	<0.01	<0.01	<0.01	<0.01	<0.01	<0.01	n.d.	n.d.	0.04
Total	100	0.30	0.26	0.28	0.56	93.5	0.19	0.27	0.10	0.86
<i>Cations</i>										
Si	1.970	2.983	1.972	0.996	0.001	0.001	2.005	1.990	2.793	6.392
Ti	0.001	0.001	0.001	<0.001	0.082	0.082	0.001	0.001	0.017	0.012
Al	0.033	1.902	0.037	<0.001	0.107	0.107	0.052	0.022	1.456	2.419
Cr	0.003	0.041	0.001	<0.001	0.267	0.267	0.012	0.001	0.017	0.104
Fe ³⁺	0.050	0.093	0.017	0.009	1.461	1.461	<0.001	<0.001	<0.001	0.111
Fe ²⁺	0.042	0.814	0.271	0.313	0.942	0.942	0.138	0.359	0.403	0.789
Mg	0.933	1.688	1.683	1.670	0.114	0.114	0.857	1.611	2.295	3.324
Mn	0.003	0.062	0.007	0.005	0.008	0.008	0.004	0.007	0.001	0.017
Ni	<0.001	<0.001	0.001	0.005	0.008	0.008	<0.001	—	—	—
Ca*	0.937	0.413	0.008	<0.001	0.009	0.009	0.855	0.009	0.000	1.635
Na*	0.027	0.002	0.001	0.001	0.001	0.001	0.076	0.001	0.072	0.196
Na†	—	—	—	—	—	—	—	—	—	0.497
K†	<0.001	<0.001	<0.001	<0.001	<0.001	<0.001	<0.001	—	0.871	—
Total	3.999	7.999	4.000	2.999	3.000	3.000	4.000	3.999	7.925	15.497

(continued)

Table 3: (Continued) Endmember proportions from wall rock garnet-peridotite (zone 1a & b, gb) and phlogopite-garnet-websterite (zone 4 and 5)

Zone:	1a and b										4 and 5														
	Garnet-peridotite (gp, cgp)										(Coarse-grained Phl-)Grt-websterite (cpgw, pgw, gw)														
Rock:	Garnet-peridotite (gp, cgp)					Garnet-peridotite (gp, cgp)					Garnet-peridotite (gp, cgp)					(Coarse-grained Phl-)Grt-websterite (cpgw, pgw, gw)									
Mineral:	Cpx	Grt	Opx	Ol	Mt	Cpx	Grt	Opx	Ol	Mt	Cpx	Grt	Opx	Phl	Amph	Cpx	Grt	Opx	Phl	Amph					
Grains (n):	9	SD	12	SD	5	9	SD	134	SD	5	5	SD	51	SD	5	5	SD	7	SD	4	5	SD	109	SD	5
Analyses (n):	91	134	51	31	5	91	134	51	31	5	117	142	109	25	5	117	142	109	25	5					
<i>Endmembers</i>																									
Fo	—	—	—	—	—	—	—	—	—	—	—	—	—	—	—	—	—	—	—	—	—	—	—	—	
En	48.8	—	—	—	—	—	—	—	—	—	—	—	—	—	—	—	—	—	—	—	—	—	—	—	
Fs	2.2	—	—	—	—	—	—	—	—	—	—	—	—	—	—	—	—	—	—	—	—	—	—	—	
Wo	49.0	—	—	—	—	—	—	—	—	—	—	—	—	—	—	—	—	—	—	—	—	—	—	—	
Di-Hed	96.1	—	—	—	—	—	—	—	—	—	—	—	—	—	—	—	—	—	—	—	—	—	—	—	
Jd	1.4	—	—	—	—	—	—	—	—	—	—	—	—	—	—	—	—	—	—	—	—	—	—	—	
Ac	2.5	—	—	—	—	—	—	—	—	—	—	—	—	—	—	—	—	—	—	—	—	—	—	—	
Py	—	56.7	—	—	—	—	—	—	—	—	—	—	—	—	—	—	—	—	—	—	—	—	—	—	
Alm	—	27.3	—	—	—	—	—	—	—	—	—	—	—	—	—	—	—	—	—	—	—	—	—	—	
Gr	—	13.9	—	—	—	—	—	—	—	—	—	—	—	—	—	—	—	—	—	—	—	—	—	—	
Spess	—	2.1	—	—	—	—	—	—	—	—	—	—	—	—	—	—	—	—	—	—	—	—	—	—	
Phl	—	—	—	—	—	—	—	—	—	—	—	—	—	—	—	—	—	—	—	—	—	—	—	—	
Mt	—	—	—	—	—	—	—	—	—	—	—	—	—	—	—	—	—	—	—	—	—	—	—	—	
Cr	—	—	—	—	—	—	—	—	—	—	—	—	—	—	—	—	—	—	—	—	—	—	—	—	
Sp	—	—	—	—	—	—	—	—	—	—	—	—	—	—	—	—	—	—	—	—	—	—	—	—	
Ab	—	—	—	—	—	—	—	—	—	—	—	—	—	—	—	—	—	—	—	—	—	—	—	—	
An	—	—	—	—	—	—	—	—	—	—	—	—	—	—	—	—	—	—	—	—	—	—	—	—	
Or	—	—	—	—	—	—	—	—	—	—	—	—	—	—	—	—	—	—	—	—	—	—	—	—	
Mg#	0.957	0.675	0.861	0.842	0.108	0.957	0.675	0.861	0.842	0.108	0.957	0.675	0.861	0.842	0.108	0.957	0.675	0.861	0.842	0.108	0.957	0.675	0.861	0.842	

(continued)

Table 3: (Continued) Average EMP measurements from garnetite (zone 6), eclogite (zone 7a) and retro-omphacite (zone 7c) in metasomatic veins in the Svartberget peridotite body

Zone:	6b				7a				7c			
	Garnetite (g)				Eclogite (e)				Retrogressed omphacite (ro)			
Mineral:	Grt	Phl	Cpx	Opx	Cpx	Grt	Cpx	Grt	Cpx	Plag	Cpx	Amph
Grains (n):	5	2	1	3	1	1	1	1	3	5	3	1
Analyses (n):	58	2	1	56	1	1	1	1	3	3	3	5
<i>Oxides (wt %)</i>												
SiO ₂	40.4	0.42	53.6	55.3	0.31	40.2	54.8	40.2	53.1	0.24	67.2	43.3
TiO ₂	0.03	0.01	0.01	0.01	0.01	0.09	0.05	0.09	0.34	0.08	0.01	0.78
Al ₂ O ₃	22.5	0.23	0.96	0.76	0.05	22.3	16.4	22.3	3.71	0.53	20.9	11.6
Cr ₂ O ₃	0.06	0.02	0.06	0.02	0.06	0.05	0.02	0.05	0.02	0.02	<0.01	<0.01
FeO	17.9	1.90	3.71	15.2	0.27	18.8	4.36	18.8	8.21	0.65	0.13	10.51
MgO	14.1	1.09	16.7	28.3	0.16	12.0	5.67	12.0	11.5	0.62	<0.01	14.93
MnO	1.03	0.12	0.06	0.32	0.01	0.72	0.07	0.72	0.21	0.04	<0.01	0.25
NiO	<0.01	<0.01	0.12	0.05	0.07	—	—	—	<0.01	<0.01	<0.01	0.00
CaO	4.52	0.74	23.7	0.29	0.02	6.28	10.0	6.28	18.5	0.96	1.43	10.8
Na ₂ O	0.05	0.06	0.57	0.12	0.16	0.06	8.86	0.06	3.86	0.30	10.62	4.46
K ₂ O	<0.01	<0.01	0.01	<0.01	<0.01	0.01	0.02	0.01	0.01	0.01	0.02	0.04
Total	101	0.14	99.5	100	0.29	101	100	101	99.4	0.16	100	96.6
<i>Cations (p.f.u.)</i>												
Si	2.968	2.787	1.960	1.974	1.931	2.985	1.931	2.985	1.945	2.933	2.933	6.342
Ti	0.002	0.079	<0.001	<0.001	0.001	0.005	0.001	0.005	0.010	<0.001	<0.001	0.086
Al	1.954	1.394	0.042	0.032	0.683	1.956	0.683	1.956	0.160	1.074	1.074	2.008
Cr	0.003	0.006	0.002	0.001	0.001	0.003	0.001	0.003	0.001	<0.001	<0.001	<0.001
Fe ³⁺	0.110	<0.001	0.077	0.027	0.088	0.069	0.088	0.069	0.205	<0.001	<0.001	0.112
Fe ²⁺	0.994	0.451	0.037	0.428	0.041	1.101	0.041	1.101	0.047	0.005	0.005	1.174
Mg	1.541	2.223	0.911	1.508	0.298	1.327	0.298	1.327	0.629	<0.001	<0.001	3.261
Mn	0.064	0.002	0.002	0.010	0.002	0.045	0.002	0.045	0.007	<0.001	<0.001	0.031
Ni	<0.001	0.007	0.003	0.002	<0.001	<0.001	<0.001	<0.001	<0.001	<0.001	<0.001	<0.001
Ca*	0.356	<0.001	0.927	0.011	0.379	0.500	0.379	0.500	0.724	0.067	0.067	1.693
Na*	0.007	0.084	0.040	0.008	0.606	0.008	0.606	0.008	0.274	0.899	0.899	0.293
Na†	—	—	—	—	—	—	—	—	—	—	—	0.972
K†	<0.001	0.884	<0.001	<0.001	0.001	0.001	0.001	0.001	<0.001	0.001	0.001	0.008
Total	8.000	7.918	3.999	4.000	4.029	4.000	4.029	4.000	4.000	4.979	4.979	15.980

Table 3: (Continued) Endmember proportions from garnetite (zone 6), eclogite (zone 7a) and retro-omphacite (zone 7c)

Zone:	6b				7a				7c					
	Garnetite (g)				Eclogite (e)				Retrogressed omphacite (ro)					
Rock:	Grt	Phl	Cpx	Opx	Cpx	Opx	Grt	Cpx	Plag	Amph	Grt	Cpx	Plag	Amph
Mineral:														
Grains (n):	5	SD	1	SD	1	SD	1	SD	1	SD	1	SD	5	SD
Analyses (n):	58	2	1	56	1	1	1	1	3	1	3	5	3	5
<i>Endmembers</i>														
Fo	—	—	—	—	—	—	—	—	—	—	—	—	—	—
En	—	—	48.6	77.5	—	—	—	—	—	—	—	44.9	—	—
Fs	—	—	1.96	22.0	—	—	—	—	—	—	—	3.34	—	—
Wo	—	—	49.4	0.57	—	—	—	—	—	—	—	51.8	—	—
Di-Hed	—	—	94.1	—	50.9	—	—	—	—	—	—	74.5	—	—
Jd	—	—	2.02	—	42.9	—	—	—	—	—	—	14.6	—	—
Ac	—	—	3.84	—	6.2	—	—	—	—	—	—	10.9	—	—
Py	52.1	—	—	—	—	—	44.6	—	—	—	—	—	—	—
Alm	33.6	—	—	—	—	—	37.0	—	—	—	—	—	—	—
Gr	12.1	—	—	—	—	—	16.8	—	—	—	—	—	—	—
Spess	2.18	—	—	—	—	—	1.53	—	—	—	—	—	—	—
Phl	—	83.1	—	—	—	—	—	—	—	—	—	—	—	—
Mt	—	—	—	—	—	—	—	—	—	—	—	—	—	—
Cr	—	—	—	—	—	—	—	—	—	—	—	—	—	—
Sp	—	—	—	—	—	—	—	—	—	—	—	—	—	—
Ab	—	—	—	—	—	—	—	—	—	—	—	—	92.9	—
An	—	—	—	—	—	—	—	—	—	—	—	—	6.92	—
Or	—	—	—	—	—	—	—	—	—	—	—	—	0.14	—
Mg#	0.608	0.831	0.961	0.779	0.880	0.931	0.547	0.931	—	—	—	—	—	0.735

Ferric iron estimated using stoichiometric methods of Droop (1987). SD, standard deviation; n.d., not determined.

*Ca and Na on B site in amphibole.

†Ca and Na on A site in amphibole [following method outlined by Leake *et al.* (1997)].

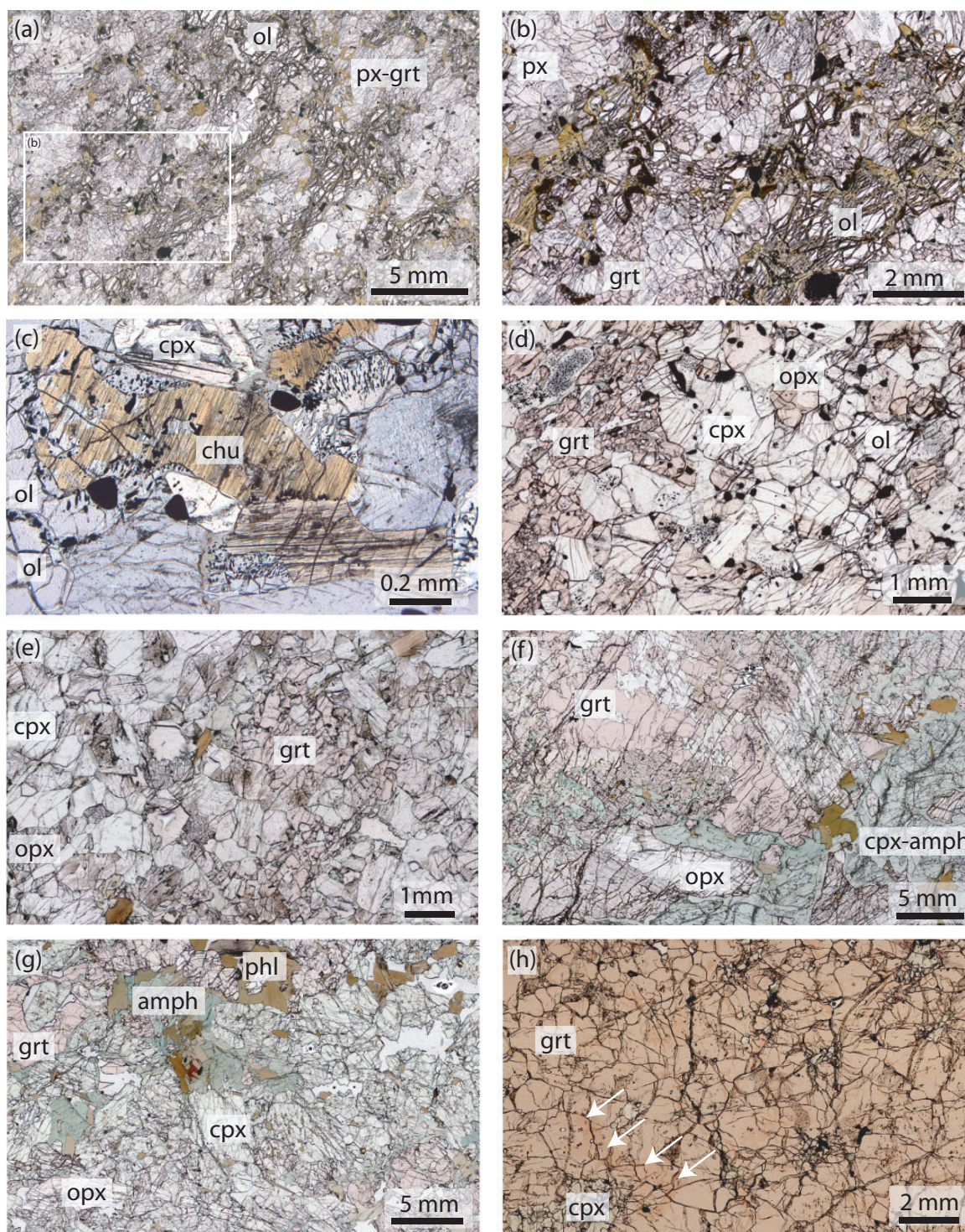


Fig. 4. Photomicrographs illustrating the most important textural features of the main zones described in the text. (a) Network-like olivine patches in a garnet–pyroxene matrix of the least metasomatized peridotite (zone 1a, gp). (b) Close-up of (a) showing microtextures of garnet and pyroxenes. The dark gray mineral around olivine is formed by late-stage alteration. (c) Late-stage breakdown of clinohumite to olivine and oxides (zone 1b; cgp). (d) Oxide-bearing olivine-websterite with equilibrium textures of orthopyroxene and clinopyroxene and interstitial poikilitic garnet (zone 1c, ow). (e) Garnet-websterite (zone 2, gw). In contrast to olivine-websterite (zone 1c, ow) oxides are absent, whereas phlogopite begins to develop. (f) Coarse-grained phlogopite–garnet-websterite (zone 4, cpwg) with very coarse-grained phlogopite, garnet and orthopyroxene occurring together with clinopyroxene that develops thick rims of amphibole. (g) Phlogopite–garnet-websterite (zone 5a, pgw) with a smaller grain size than that of zone 4. (h) Garnetite (zone 6b, g), with minor clinopyroxene inclusions in garnet, shows slightly darker veining indicated by white arrows. Abbreviations: ol, olivine; px, pyroxene; grt, garnet; opx, orthopyroxene; cpx, clinopyroxene; chu, clinohumite; amph, amphibole.

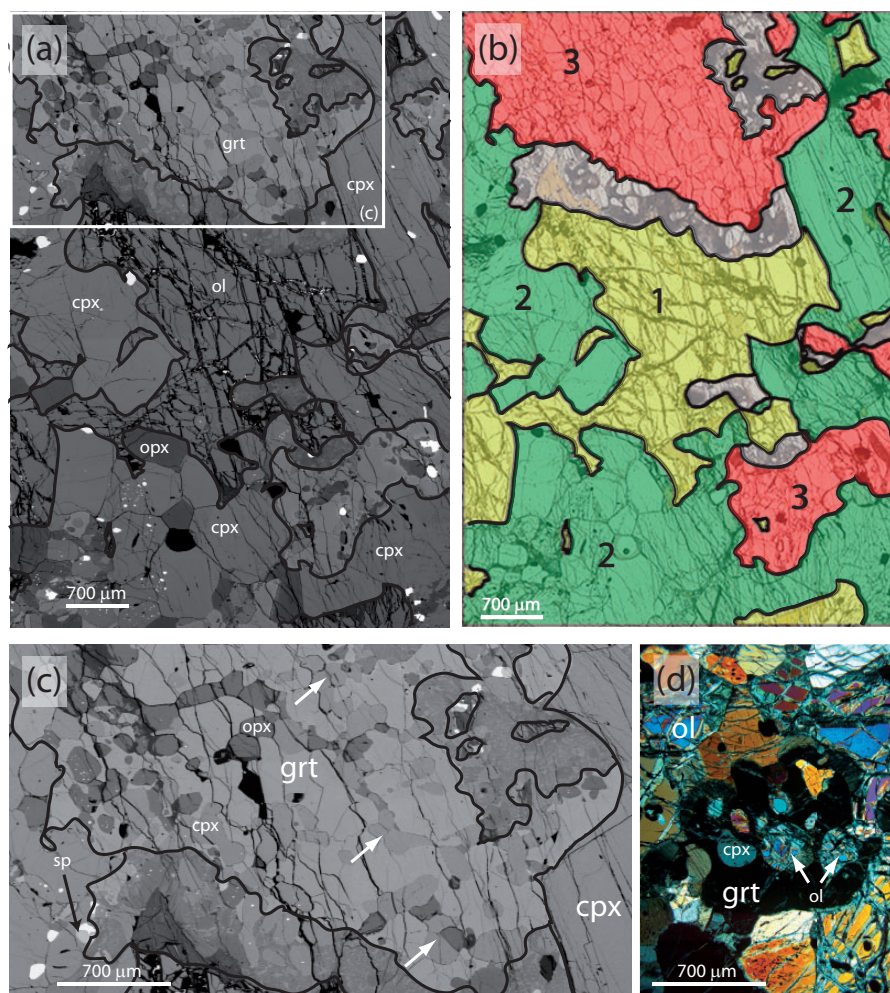


Fig. 5. Microtextures in a sample from the most pristine rock zone (zone 1a, gp). (a) Back-scattered electron image of large olivine crystals with resorption features indicated by a corrosive shape and convex grain boundaries. Clinopyroxene and orthopyroxene have mainly concave grain boundaries with olivine, whereas they form equilibrium textures with 120° angles where they are in contact to each other. Garnet forms large poikilitic grains with irregular, mainly concave grain boundaries. (b) shows the three textural domains recognized in (a), numbered by the timing of their formation: 1, olivine dominated; 2, pyroxene dominated; 3, garnet dominated. The grey parts have been affected by late-stage alteration. (c) Magnification of the upper part of (a) showing poikilitic garnet with rounded pyroxene inclusions (medium grey, Cpx; dark grey, Opx) with locally preserved equilibrium grain boundaries (white arrows). The black arrow in the lower-left corner indicates spinel associated with primary Fe–Ti oxides. (d) Photomicrograph showing that the poikilitic garnet is an interstitial phase that has replaced former pyroxene and olivine (see Supplementary Data Fig. 4 for back-scattered electron image).

coarse-grained crystals commonly with inclusions of orthopyroxene and clinopyroxene and occasionally phlogopite.

Primary veins

The primary veins consist of a variety of coarse-grained phlogopite–garnet–websterite zones (zone 5). The cores of these veins are mostly filled with garnetite (zone 6), but in some localities with eclogite (zone 7; Fig. 3c) and pegmatite (zone 8; Fig. 3d).

Zone 5 (*diamond-bearing grt-websterite*)

Zone 5a: pgw. This zone is the outermost zone in the veins and has the same mineral assemblage as zone 4 (Figs 2c

and 3a). It differs in two aspects: it is finer grained and it has a more regular width and therefore clearly marks the outermost zone of the veins.

Samples are green, undeformed and consist of subhedral to euhedral, medium- to coarse-grained (1 mm to 1 cm), unoriented crystals. The rocks consist roughly of 45–60% clinopyroxene, 5–30% orthopyroxene, 10% phlogopite and 5–10% garnet with accessory amphibole and apatite. Polyphase solid inclusion assemblages are omnipresent in garnet and some contain diamond (Vrijmoed *et al.*, 2008). Mineral textures and shapes, and the overall structure of the rock in thin section, are similar to those of the previously described zone (zone 4),

apart from the more homogeneous and smaller grain size (Fig. 4g).

Zone 5b: phlogopite-free garnet-websterite, pfgw. Moving towards the core of the veins, this zone consists of garnet-websterite and has the same characteristics as the previous zone (zone 5a), except for the absence of phlogopite (Fig. 3a). It is found in close relation with the garnetites (described in the next two zones, 6a and b). The width of the zone is usually <5 mm.

Zone 6 (garnetite)

In 95–99% of occurrences this zone represents the core of the primary veins (Fig. 3a and b). At one location the garnetite core of a 3 m wide coarse-grained phlogopite–garnet-websterite, zone 4, consists of two distinct zones described below.

Zone 6a: inclusion-bearing garnetite, ig. Garnetite in this zone is similar to the garnetite described in detail below for the next zone (g, zone 6b), except for the presence of inclusion-rich garnet (Fig. 3b). Although a detailed investigation of these inclusions has not been performed, inclusions of ortho- and clinopyroxene seem to be the dominant type. This zone is observed only in the southern part of the coarse-grained phlogopite–garnet-websterites.

Zone 6b: garnetite ± phlogopite. Garnetite of this zone is 5–10 cm in width; it outlines the primary vein system crosscutting the Svartberget peridotite body, and is always observed in the core of phlogopite–garnet-websterites (zones 4 and 5; see Figs 1, 2b, c and 3a, b). Garnetite generally is confined to narrow veins even where they occur in zone 4, where the phlogopite–garnet-websterite zones are wide and irregular. Locally it can have more complex pod-like or other more irregular shapes that are often discontinuous, as can be seen in detail on the map (4–5 locations in the outcrop; see Suppl. Data Fig. 1). In veins around at least three blocks (from the 710 mapped blocks), garnetite is found with a core zone of phlogopite. Samples of garnetite are undeformed, homogeneous and characteristically red. Garnetite typically comprises 97% garnet, 1% phlogopite, 1% orthopyroxene and 1% clinopyroxene. Apatite, monazite, zircon, rutile and ilmenite are present as accessory phases. Patchy structures marked by differences in red colour intensity appear in thin section and represent slight compositional variations (Fig. 4h, Suppl. Data Fig. 3h). The grains appear to be subhedral and equigranular, varying from medium to coarse grained. Micrometre-sized fluid inclusion trails are present and cross grain boundaries. Anhedral orthopyroxene or clinopyroxene grains are interstitial to the garnet grains. Phlogopite is present as clusters of randomly oriented, subhedral, lenticular grains or as veins in some thin sections. Rutile, apatite and ilmenite with lamellae of hematite form anhedral inclusions in garnet.

Zone 7 (eclogite)

An eclogite zone is present in the core of garnetite in at least four to five localities in the studied outcrop (Fig. 3c, with details in Fig. 6). This zone consists of three sub-zones: 7a, eclogite; 7b, retrograde eclogite; 7c, retrograde omphacitite (with <1% grt).

Zone 7a: eclogite, e. Between garnetite and the core of the veins a thin (1 mm) zone of eclogite is preserved; the jadeite contents of the clinopyroxene reach ~30% (Table 3).

Zone 7b: retrograde eclogite, re. The rim of the eclogite zone is retrogressed to an undeformed, homogeneously very fine-grained, black to dark green, 5 mm thick zone. A symplectitic intergrowth of amphibole (±50%) plagioclase (±50%) and magnetite (<1%) is characteristic for this zone in thin section.

Zone 7c: retrograde omphacitite, ro. Locally, the garnetite core is filled with a homogeneous, fine-grained, milky-green, symplectitic rock. Slightly elongated, millimetre-sized, oriented domains of similar extinction consist of hundreds of grains and suggest the former presence of coarser-grained omphacite or jadeite. The rock is undeformed and now comprises approximately 35% amphibole, 25% clinopyroxene, 35% plagioclase and 5% garnet in micrometre-sized, anhedral, symplectitic intergrowth. Zircon and apatite are common accessories. Minor garnet, rimmed by retro-eclogite (dark amphibole-rich rim, zone 7b), occurs locally inside the zone.

Zone 8 (pegmatite, peg)

Three to four of the eclogite localities have a core of amphibole–plagioclase pegmatite (Fig. 3d). Here, the retrogressed omphacitite hosts pegmatite consisting of euhedral, coarse-grained (grain size 1–5 cm) plagioclase, quartz, amphibole, clinopyroxene and apatite. Plagioclase is sericitized and amphibole is locally symplectitic and intergrown with plagioclase and quartz. It is important to note that this rock type is found in the middle of veins and does not crosscut the veins like many other pegmatites that can be followed into the surrounding gneiss. The pegmatite in this zone differs from other, more regular, pegmatites found in the host gneiss in having amphibole and (diopsidic) clinopyroxene as constituent minerals.

Immature primary veins

Within several blocks of wall-rock peridotite thin (≤ 5 cm) websterite, garnetite and phlogopite zones occur that are referred to as ‘immature’ zones. These zones have the same mineralogy as the peridotite wall-rock (Suppl. Data Fig. 3). They are characterized by an enrichment zone of clinopyroxene with a core zone enriched in phlogopite and garnet. These zones are interpreted as regions where garnetite (±phlogopite) (zone 6) and websterite (zone 4 and 5) mineral assemblages have not fully developed to form the primary veins described above. In thin section it

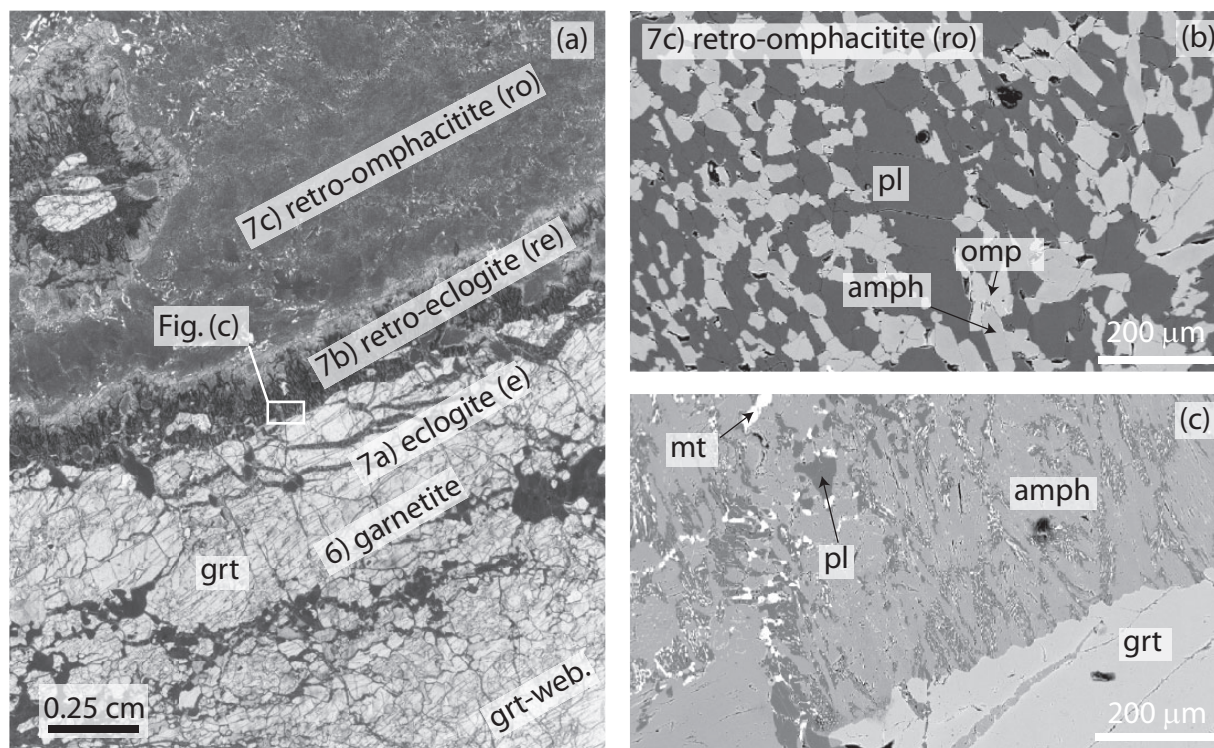


Fig. 6. (a) Photomicrograph detailing the transition from phlogopite-free garnet-websterite (zone 5b, pfgw) to eclogitic garnetite (zone 7a, e) and the retrograde omphacitite (zone 7c, ro) that fills the central part of the former fracture. The clinopyroxene in the garnet-websterite (pfgw) becomes more sodic toward the garnetite and is transformed into omphacite within the garnetite (zone 6). (b) The retrograde omphacitite now consists of an intergrowth of albite plagioclase (pl), amphibole (amph), and omphacite (omp). (c) Retrogressed contact (zone 7b, re) between eclogite-garnetite and omphacitite. All previously existing omphacite is converted into an intergrowth of albite plagioclase and amphibole.

can be seen that the zones lack the oxides that are characteristic of the wall-rock and some olivine remains.

Secondary veins and retrogression

Retrogression of the Svartberget body is restricted to narrow zones along subparallel, subvertical fracture systems and minor amphibole in rims around garnet and clinopyroxene (see modes listed above and in Table 1). Zones consisting mainly of amphibole, chlorite and talc, with sharp lithological contacts, are discordant to and crosscut all previously described zones and are usually ~0.5 cm, occasionally 15–20 cm, wide (Fig. 3d). Locally these zones cause penetrative alteration of the peridotite body, and we refer to them as secondary veins and consequently altered versions of all primary zones. The penetrative alteration also occurs at the contact with the host-rock gneiss and is clearly related to late-stage pegmatites that can be followed from the local country rock into the Svartberget body. As described above, these pegmatites differ from zone 8 pegmatites in that amphibole and clinopyroxene have not been found. Zones that are 15–20 cm wide have thin (<1 cm) pegmatite veins in the core that

do not vary in width. The strike of the veins is approximately north–south, but numerous thin, pegmatite-free, alteration zones deviate from this direction by up to 10°. In total these secondary zones of retrogression are restricted to less than 3% of the total outcrop (Table 1).

Host-rock migmatitic gneiss

Samples were taken from leucosomes and the host-rock gneiss for whole-rock geochemical and strontium isotope analysis and zircon geochronology. The leucosomes are coarse grained, usually unfoliated, and consist of plagioclase, K-feldspar and quartz with minor biotite. The gneiss itself is strongly foliated, medium grained, and consists of plagioclase, K-feldspar, biotite, amphibole and quartz. Sillimanite is observed a few hundreds of meters away from the Svartberget body and, locally, fine-grained garnet is present in the gneiss.

ANALYTICAL METHODS

Whole-rock major and trace element measurements were performed on homogenized (agate ball mill) powders

using a Philips PW 2400 X-ray spectrometer, following standard methods at the Faculty of Earth and Life Sciences, VU University, Amsterdam. The sample sizes spanned the width of the metasomatic zones in typical hand specimen sizes ($\sim 10\text{ cm}^3$). To resolve the composition in the zones, and ensure representativity, the sample sizes were smaller for the narrow finer-grained zones than for the wider coarse-grained zones. A mixture of 66% Li-tetaborate and 34% Li-metaborate were added to the beads for measurement of the major elements. Where possible calibration curves for trace elements are determined using samples whose compositions had previously been characterized by isotope dilution (Rb, Sr, U, Pb, Th, REE, Zr, Hf) to ensure accuracy of low concentration measurements down to 1 ppm. International standards used to validate the authenticity of the analysis were AGV-1, BCR-2, BHVO-2 and GSP-1 (Suppl. Data Table 1). Below that level, owing to lower counting statistics, errors are higher ($\pm 10\%$); below 0.5 ppm analyses are semi-quantitative, below 0.1 ppm $\pm 50\%$, and below 0.05 ppm meaningless. The major element analyses of the standards are all within 1% of the accepted values, as are Sr, Y, Zr, Nb, Ga, Zn, V, and Cu. Other trace elements appear less accurate compared with accepted standard data; Rb <2%, Ba and Pb <3%, Ni and La <4% and Sc, Cr and Yb <6%.

Mineral compositions were analyzed using a Cameca SX-100 electron microprobe (EMP) at the University of Oslo, using an accelerating voltage of 15 kV, a current of 15 nA and a beam diameter of $1\ \mu\text{m}$ for all minerals except for plagioclase ($10\ \mu\text{m}$). The standards were wollastonite (Si and Ca), synthetic corundum and periclase (Al and Mg), pyrophanite (MnTiO_3 for Mn and Ti), both Fe_2O_3 and Fe (metal), Cr_2O_3 , albite (Na), orthoclase (K), NiO, and fluorite (F). The matrix corrections were Cameca's standard PAP routine (Pouchou & Pichoir, 1984).

Samples for strontium isotope analysis were dissolved in a mixture of hydrofluoric and nitric acid and measured by thermal ionization mass spectrometry (TIMS) at the Faculty of Earth and Life Sciences VU University, Amsterdam using a Finnigan MAT 262 RPQ-plus instrument. Data were corrected for isotope fractionation to $^{86}\text{Sr}/^{88}\text{Sr} = 0.1194$ and the Sr standard NBS 987 ratio yielded 0.710244 ± 8 over the 2 years preceding the measurements cited here. All standards measured concurrently with our analyses are within error of this ratio.

Zircon, monazite and rutile grains were extracted from bulk-rock samples of $\sim 400\text{ cm}^3$ after crushing and pulverizing in a jaw crusher and a hammer mill and various steps of enrichment using a Wilfley table, Frantz magnetic separator and heavy liquids. They were handpicked in alcohol under a binocular microscope. All zircon and monazite separates were mechanically abraded prior to dissolution. The isotope dilution (ID)-TIMS procedure at

the University of Oslo follows standard techniques (Krogh, 1973), as described by Corfu (2004). Zircon and rutile were dissolved in HF in Teflon bombs at 184°C . Monazite was dissolved in 6N HCl in Savillex vials on a hot-plate. The U and Pb isotope analyses were corrected for blanks of $\leq 2\text{ pg Pb}$ and 0.1 pg U , respectively. The residual common Pb was subtracted using compositions estimated with the Stacey & Kramers (1975) model. The uncertainties on the ratios are given as 2σ values and were estimated by quadratic propagation of the main sources of error, including Pb isotope reproducibility of $\pm 0.06\%$ per a.m.u. for Faraday, and $\pm 0.1\%$ per a.m.u. for multiplier measurements. The results are plotted using the program Isoplot (Ludwig, 1999).

RESULTS

Whole-rock geochemistry

The whole-rock geochemical data display a trend from an original Mg- and calcium-rich composition, relatively low in fluid-mobile elements, towards a felsic and calcium-poor composition (Fig. 7). This trend is accompanied by enrichment in incompatible elements (Fig. 8) and an increase in radiogenic Sr from wall-rock (zone 1) to vein (zones 5–7). Table 2 presents data for representative samples of each zone. The complete dataset is given in Suppl. Data Tables 2–6.

Major elements

The major element variations are plotted based on field relations (from zones 1–8), organized from zone 1a to 8 and then the leucosomes, the latter representative of the host-rock gneiss (Fig. 7).

Silica concentrations generally increase from zone 1 (46.5–48.7%) to zone 8 (61.9%), with the nearly monomineralic zones 5b, 6a, b and 7a, b (dominantly clinopyroxene or garnet) being the exception. The SiO_2 concentration of garnetite (zone 6a and b; ig and g respectively) and eclogite (zone 7a and e) is controlled by garnet and thus has concentrations as low as 42.3–43.6%. When plotted in an MgO– SiO_2 diagram (Suppl. Data Fig. 6), the samples define a linear trend (with the exception of the garnetites) with the most pristine rock type (zone 1a, gp) on the high-MgO–low- SiO_2 end and leucosomes from the gneiss at the low-MgO (0.1%) and high- SiO_2 (74.9–76.9%) end.

The MgO concentrations are highest in the most pristine peridotite (zone 1a and b; gp and cgp; 25.4–27.8%) and remain above 20% throughout zones 1–3 in the peridotite blocks. Coarse-grained phlogopite–garnet–websterite from zone 4 (cpgw) that forms the transition from blocks to veins has slightly lower MgO, 20.8–23.1%. The veins are marked by a stronger decrease in MgO, dropping to 16.2% in phlogopite–garnet–websterite in zone 5a (pgw) and decreasing further to 15.8% in zone 5b (pfgw)

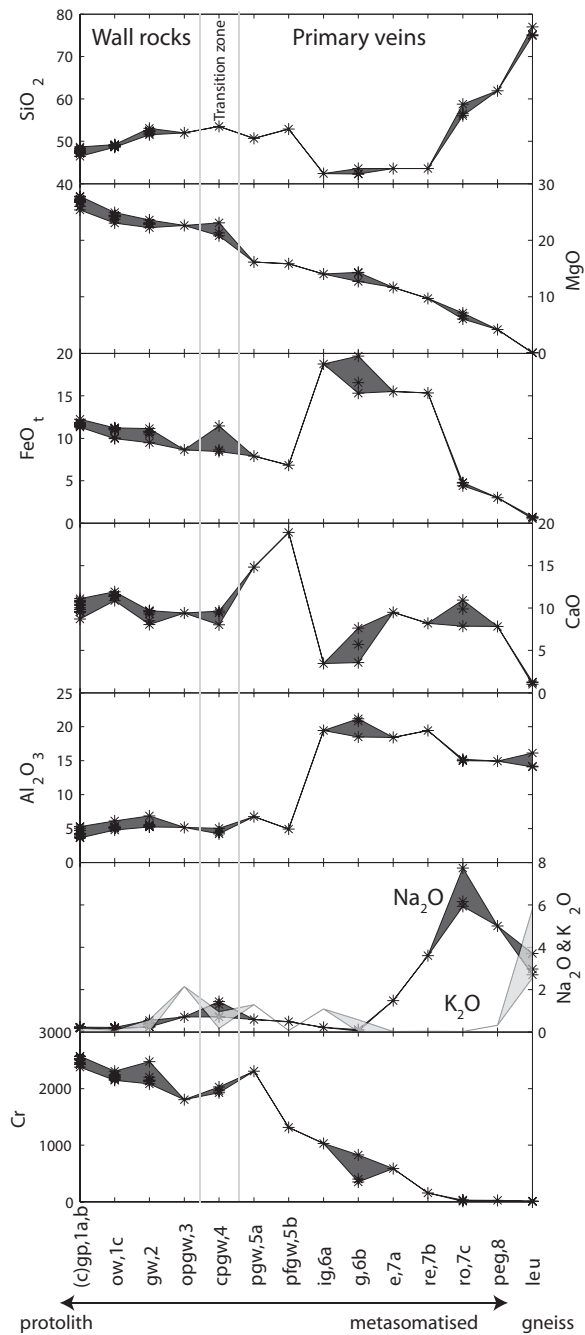


Fig. 7. Major element concentrations plotted for each rock zone, arranged from the least metasomatized rock (zone 1a, gp) to zone 8 (peg), ending with leucosomes within gneiss to the right. The plots indicate a trend from an original MgO- and calcium-rich composition, relatively depleted in fluid-mobile elements, towards a felsic, calcium-poor composition enriched in fluid-mobile elements. The concentrations of MgO and Cr, typical for mafic (or ultramafic) rocks steadily decrease from the least metasomatized rocks (zone 1a, gp) to the leucosomes (leu) whereas the incompatible elements Na₂O and K₂O typical of felsic rocks increase from zone 1 to the leucosomes. The contents of FeO and CaO decrease from the most pristine rock (zone 1a, gp) towards the leucosome, with abrupt compositional changes in the more mono- and bi-mineralic rocks in the veins: zone 5b (pfgw), 6 (ig, g) and 7 (e, re, ro). The trend is reversed for SiO₂ and Al₂O₃,

and 12.7–14.3% in garnetite in zone 6 (a and b; ig and g, respectively). A sample extracted from the thin eclogite zone (7a, e) (Fig. 6) has an MgO concentration of 11.7%. The MgO concentration decreases further in the adjacent retrogressed eclogite (zone 7b, e) to 9.7%. Finally MgO decreases to 6.1–7.1% in retrogressed omphacite, (zone 7c, ro) and is as low as 4.2% in the amphibole-bearing pegmatite (zone 8, peg).

Total iron (FeO_t) concentrations decrease from zone 1 to 8, but like SiO₂ with the exception of near mono-mineralic zones (Fig. 7). Concentrations in the garnet-peridotite (zone 1a and b; gp and cgp, respectively) are 10.2–11.0%, and decrease to 7.8–10.1% in the transition from blocks to veins (zone 4; cpgw). FeO_t decreases through the veins to 3.0% in the pegmatite (zone 8). Leucosomes have the lowest FeO_t (0.5–0.7%) concentrations. Garnetites including the eclogite and retro-eclogite (zones 6a, b and 7a, b; ig, g and e, re, respectively) have relatively high FeO_t concentrations of 13.5–17.7%.

Concentrations of CaO are more variable, but generally have spatial control from high CaO concentrations in zone 1 (8.7–11.9%, zone 1a–c) to lower concentrations in zones 2 and 3 (8.0–9.7%). Garnetite and eclogite zones (6a, b and 7a, b) follow the general trend (CaO concentrations of 3.5–9.5 wt %), in contrast to FeO_t and MgO. Retrogressed omphacite (zone 7c, ro) and amphibole pegmatite (zone 8, peg) have CaO concentrations largely overlapping (7.9–10.9%) with the garnetites. The largest outliers are zones 5a and b, with respectively 14.8 and 18.9% CaO. The CaO concentration in these samples is controlled by the mineral assemblage that consists dominantly of clinopyroxene. Leucosomes from the gneiss have the lowest CaO concentrations (1.0–1.3%).

Similar to SiO₂, Al₂O₃ concentrations are lowest (3.6–6.8%) in the wall-rock peridotite (zone 1a and b; gp and cgp, respectively), whereas leucosomes in the host-rock gneiss have the highest concentrations (14.2–16.1%). The other zones of the Svartberget body lie between these two endmembers, with the exception of the garnetite zones, which have concentrations up to ~20%. The zones consisting almost exclusively of garnet (zones 6a, b and 7a) and the thin retrogressed eclogite zone (7b, Fig. 6) have Al₂O₃ concentrations approaching those that are typical for garnet (e.g. 20–22%).

Fig. 7 Continued

again with the exception of the veins: zone 5b (pfgw), 6 (ig, g) and 7 (e, re, ro). Abbreviations: gp, garnet-peridotite; cgp, clinohumite-bearing garnet-peridotite; ow, olivine-websterite; gw, garnet-websterite; opgw, orthopyroxene-bearing phlogopite-garnet-websterite; cpgw, coarse-grained phlogopite-garnet-websterite; pgw, phlogopite-garnet-websterite; pfgw, phlogopite-free garnet-websterite; ig, inclusion-rich garnetite; g, garnetite; e, eclogite; re, retrogressed eclogite; ro, retrograde omphacite; peg, amphibole pegmatite; leu, leucosome.

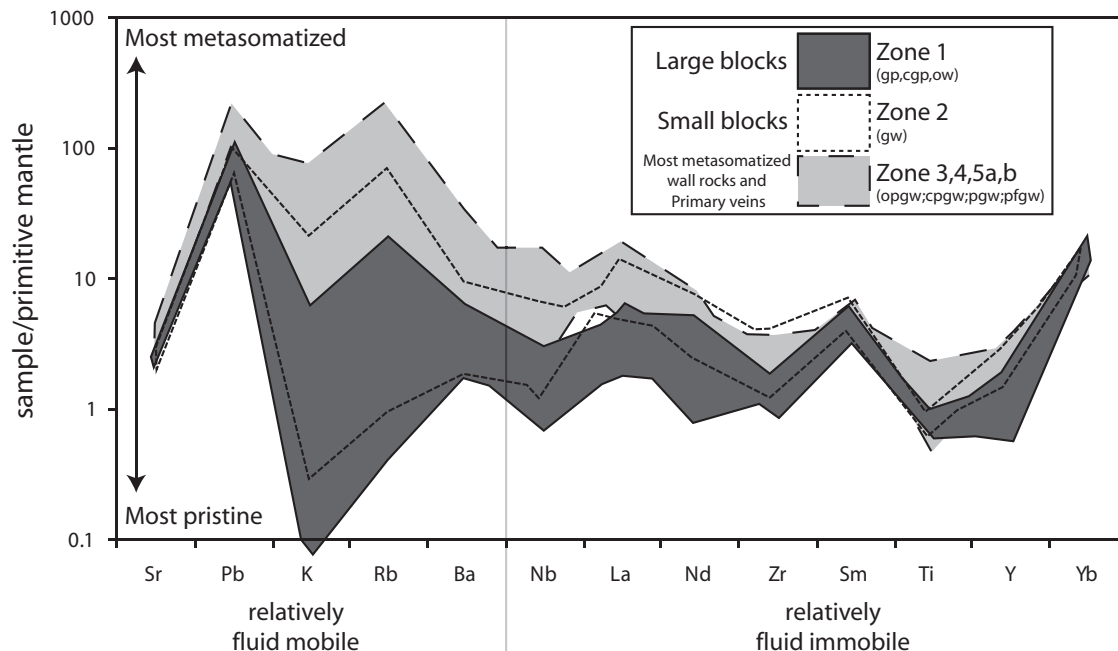


Fig. 8. Trace element data normalized to primitive mantle values (Sun & McDonough, 1989). The most fluid-mobile elements are plotted to the left, whereas the more fluid-immobile elements are plotted to the right. It is evident that the concentrations of the fluid-mobile elements increase considerably from the most pristine rock (zone 1a, gp) towards the websterite (zone 5) at the contact of the garnetites. The most incompatible, relatively fluid-immobile elements (e.g. Nb, La) also show elevated concentrations with increasing degree of metasomatism. Abbreviations: gp, garnet-peridotite; cgp, clinohumite-bearing garnet-peridotite; ow, olivine-websterite; gw, garnet-websterite; opgw, orthopyroxene-bearing phlogopite-garnet-websterite; cpgw, coarse-grained phlogopite-garnet-websterite; pgw, phlogopite-garnet-websterite; pfgw, phlogopite-free garnet-websterite.

Concentrations of Na_2O and K_2O (0.19–0.23% and $\leq 0.18\%$, respectively) are lowest in the wall-rock peridotite (zone 1a and b) and garnetites (zone 6). Both Na_2O and K_2O show an increase towards zones 3 (opgw) and 4 (cpgw). However, Na_2O and K_2O concentrations are strongly controlled by the mineral assemblages, with low amounts in garnet-rich samples (0.05–0.22 and 0.02–0.05%, respectively). For example, K_2O can increase in single samples owing to the presence of phlogopite (e.g. zone 3). Locally garnetite contains phlogopite. Both Na_2O and K_2O increase strongly toward the leucosomes as expected for felsic rocks. However, Na_2O is strongly concentrated in eclogite (zone 7, 3.6–7.7%) peaking in the retrograde omphacite (zone 7b, ro) at 5.9–7.7%, higher than in the leucosomes.

Chromium concentrations are as high as 2600 ppm in the wall-rock peridotite (zone b; cgp) but generally decrease towards the centre of the fracture; 22 ppm in zone 8 (peg).

The development of secondary zones (Suppl. Data Table 6) that locally overprint all primary zones (zone 1–8) does not appear to have caused large changes in the major element composition of the original rock, but these are slightly higher in CaO ($\pm 1\%$) and Na_2O ($\pm 0.5\%$) in (phlogopite)-garnet-websterites (zone 2, gw; zones 4 and 5, cpgw and pgw, pfgw). One overprinted garnetite is notable as it contains $\sim 2.2\%$ P_2O_5 and has a higher CaO content

than other garnetites ($\sim 2\%$). These variations are consistent with the occurrence of apatite, observed in one garnetite sample of the primary zones, suggesting that apatite is not formed by secondary overprinting. With the current dataset it is impossible to determine whether this local variation of apatite is a significant feature of the metasomatic history of the Svartberget body or if it is the result of unrepresentative sampling.

Trace elements

Trace-element concentrations are listed in Table 2 and variations are summarized in Fig. 8 where the elements are organized following the criteria of Pearce (1983). Figure 8 shows that elements that are relatively fluid-mobile (as defined by their solid-fluid partition coefficients), such as Sr, Pb, K, Rb and Ba, increase from the most pristine to the most metasomatized rock types. Rubidium increases from sub ppm values in the wall-rock peridotites to as high as 287 ppm in the core of the veins (Suppl. Data Table 5), but it can vary strongly between samples because of the variable distribution of its main host phlogopite. Strontium increases less dramatically from 44 to 94 ppm. The behaviour of compatible to moderately incompatible elements (Ni, V, Zn, Sc, Cu, and Ga) is shown in Fig. 9. For comparison, Cr is also plotted in this diagram. Chromium, Ni and V decrease from the wall-rock to the

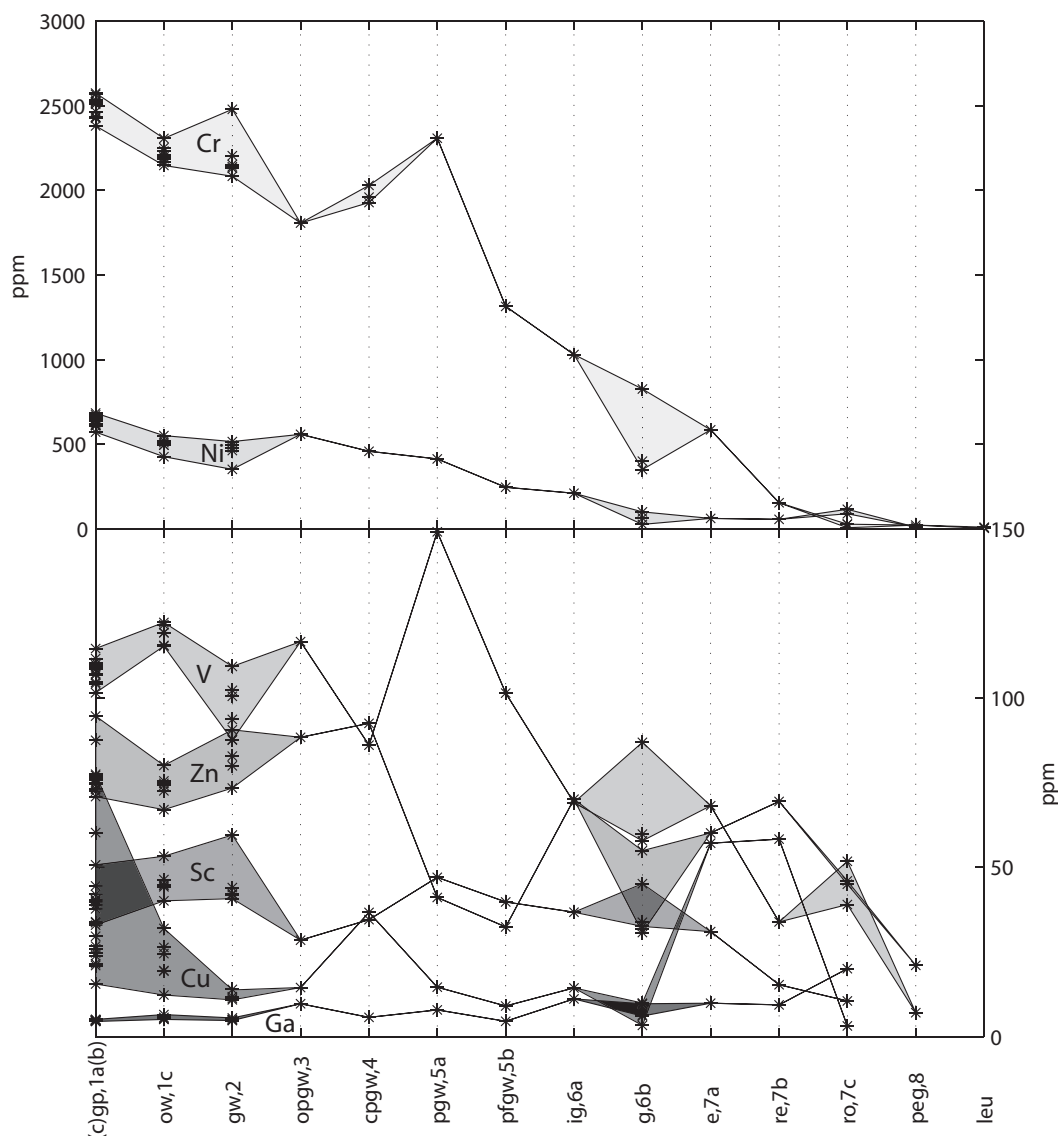


Fig. 9. Moderately incompatible elements (transition metals plus Ga) plotted against increasing degree of metasomatism. Incompatible elements Cr and Ni are plotted for comparison. Chromium, Ni, V and Cu concentrations decrease with increasing degree of metasomatism, whereas Zn and Sc concentrations remain almost constant. Only Ga shows slightly higher concentrations in the more metasomatized samples. Abbreviations: gp, garnet-peridotite; cgp, clinohumite-bearing garnet-peridotite; ow, olivine-websterite; gw, garnet-websterite; opgw, orthopyroxene-bearing phlogopite-garnet-websterite; cpgw, coarse-grained phlogopite-garnet-websterite; pgw, phlogopite-garnet-websterite; pfgw, phlogopite-free garnet-websterite; ig, inclusion-rich garnetite; g, garnetite; e, eclogite; re, retrogressed eclogite; ro, retrograde omphacite; peg, amphibole pegmatite; leu, leucosome.

core of the veins, whereas Zn, Sc and Cu concentrations are relatively constant. Chromium contents in the wall-rock are as high as 2500 ppm and decrease to 350 ppm in garnetite and 26 ppm in retrogressed eclogite. Vanadium in phlogopite-garnet-websterite (pgw, zone 5a) shows a marked deviation from this trend. Concentrations of high field strength elements, such as Zr and Nb, strongly increase in the core of veins compared with the wall-rock; from 9 to 270 ppm and from <1 to 23 ppm, respectively.

Mineral chemistry

Table 3 lists average mineral compositions for the most important minerals in selected zones that show the largest variation in lithology: wall-rock peridotite (zone 1a, gp), phlogopite-garnet-websterite (zone 5a, pgw), garnetite (zone 6, g), eclogite (zone 7a) and retrograde omphacite (zone 7c). Figure 10 shows how the changes in bulk-rock chemistry are reflected in the mineral abundance and composition.

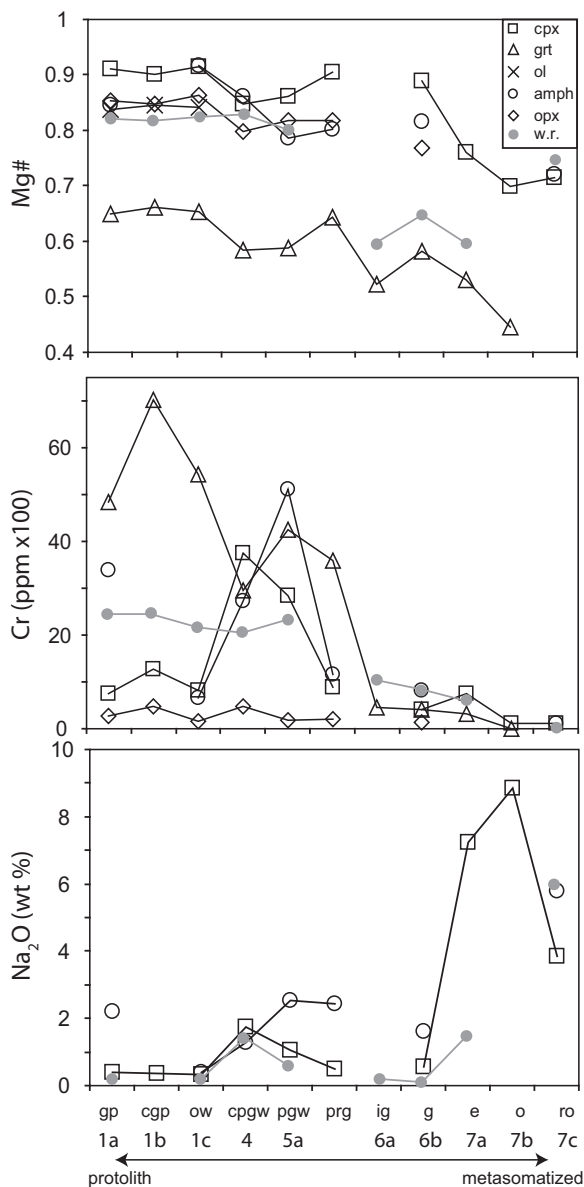


Fig. 10. Variations of mineral chemistry vs degree of metasomatism. All minerals become more Mg-poor with increasing metasomatism. Garnet, clinopyroxene, and amphibole display decreasing Cr_2O_3 contents towards the most altered rocks, with a positive excursion within the various websterites. The Na_2O concentrations in amphibole and most significantly in clinopyroxene increase with increasing degree of metasomatism. Abbreviations: gp, garnet-peridotite; cgp, clinohumite-bearing garnet-peridotite; ow, olivine-websterite; cpgw, coarse-grained phlogopite-garnet-websterite; pgw, phlogopite-garnet-websterite; prg, premature garnetite; ig, inclusion-rich garnetite; g, garnetite; e, eclogite; o, omphacite preserved inclusion; ro, retrograde omphacite.

Magnetite ($\text{Mt}_{80}\text{Cr}_{14}\text{Spl}_6$) in the wall-rock peridotite (zone 1a and b; gp and cgp) is Cr-rich and has an Mg number of 0.11. Olivine (Fo_{84}) in the wall-rock disappears in the veins reflecting the silica increase. Orthopyroxene becomes more Fe-rich and Mg-poor from the wall-rock

into the fracture ($\sim\text{En}_{85}\text{Fs}_{14}\text{Wo}_{0.4}$ to $\sim\text{En}_{78}\text{Fs}_{22}\text{Wo}_{0.6}$). Clinopyroxene varies from $\sim\text{En}_{49}\text{Fs}_2\text{Wo}_{49}$ in the wall-rock, to $\sim\text{En}_{46}\text{Fs}_8\text{Wo}_{46}$ in websterite, back to $\sim\text{En}_{49}\text{Fs}_2\text{Wo}_{49}$ in garnetite, ending with $\sim\text{En}_{45}\text{Fs}_3\text{Wo}_{52}$ in the retrogressed eclogite, and therefore follows only in part the trend towards more Fe-rich (Mg-poor) compositions. Sodium in clinopyroxene increases from ~ 0.39 wt % Na_2O corresponding to $\text{Jd}_{1.4}$ in wall-rock peridotite to ~ 8.85 wt % Na_2O (Jd_{43}) in eclogite (except in garnetite).

Garnet becomes more Fe-rich towards websterite ($\text{Py}_{57}\text{Alm}_{27}\text{Gr}_{14}\text{Sp}_{52}-\text{Py}_{50}\text{Alm}_{35}\text{Gr}_{13}\text{Sp}_{52}$) but its Fe content decreases in garnetite ($\text{Py}_{56}\text{Alm}_{29}\text{Gr}_{13}\text{Sp}_{52}$). Phlogopite occurs in websterite and garnetite and increases slightly in FeO content from Phl_{85} to Phl_{83} . The same trend in Fe increase characterizes the amphibole, which occurs as rims around clinopyroxene in websterite (Mg number 0.81) and in retro-eclogite (Mg number 0.74). Similar to the clinopyroxene, amphibole increases in Na_2O content from tschermakitic amphibole in websterite to taramitic in retro-eclogite. Plagioclase in retro-eclogite is albite ($\text{Ab}_{93}\text{An}_{6.9}\text{Or}_{0.1}$).

Mineral-chemical variation

A characteristic feature of the mineral chemistry in the Svartberget peridotite is a phenomenon we refer to as 'veining'. This veining is marked by sharp compositional contrasts within single grains that record complex vein-like or patchy compositional variations that contrast with the regular core-rim zonation that characterizes many metamorphic minerals. It is similar to observations made by Spandler *et al.* (2011). The veining is defined by variations of (1) Cr_2O_3 in garnet from peridotite (zone 1a, gp) and websterite (zone 5a, pgw), and Cr_2O_3 -FeO-MgO in garnet of garnetite (zone 6b, g); (2) Cr_2O_3 in clinopyroxene from peridotite (zone 1a, gp) and websterite (zone 5a, pgw); and (3) Al_2O_3 in orthopyroxene from websterite (zone 5a, pgw). Examples are shown in Fig. 11.

Garnet in peridotite (zone 1a, gp) has Cr_2O_3 contents that vary from 0.28 to 1.85 wt % and can vary from 0.55 to 1.70 wt % within single grains by means of sharp compositional contrasts (Fig. 11a and b). In websterite (zone 5a, pgw), garnet Cr_2O_3 varies from 0.31 to 1.25 wt % (0.68–1.25 wt % within single crystals). In contrast, Cr_2O_3 contents in garnet from garnetite (zone 6b, g) are low and vary from 0 to 0.15 wt % between and within grains. Locally, garnet from the inclusion-rich garnetite zone (zone 6a, ig) displays a concentric zoning with the lowest Cr_2O_3 and MgO contents in the inclusion-rich core and the highest Cr_2O_3 and FeO contents in the inclusion-free rim (Suppl. Data Fig. 7). Additionally, CaO decreases in the rim from ~ 4 to ~ 3.5 wt % whereas MnO increases slightly from ~ 1.06 to ~ 1.64 wt % (Suppl. Data Fig. 7). These compositional features have not been observed in garnet of the inclusion-free garnetite (zone 6b,

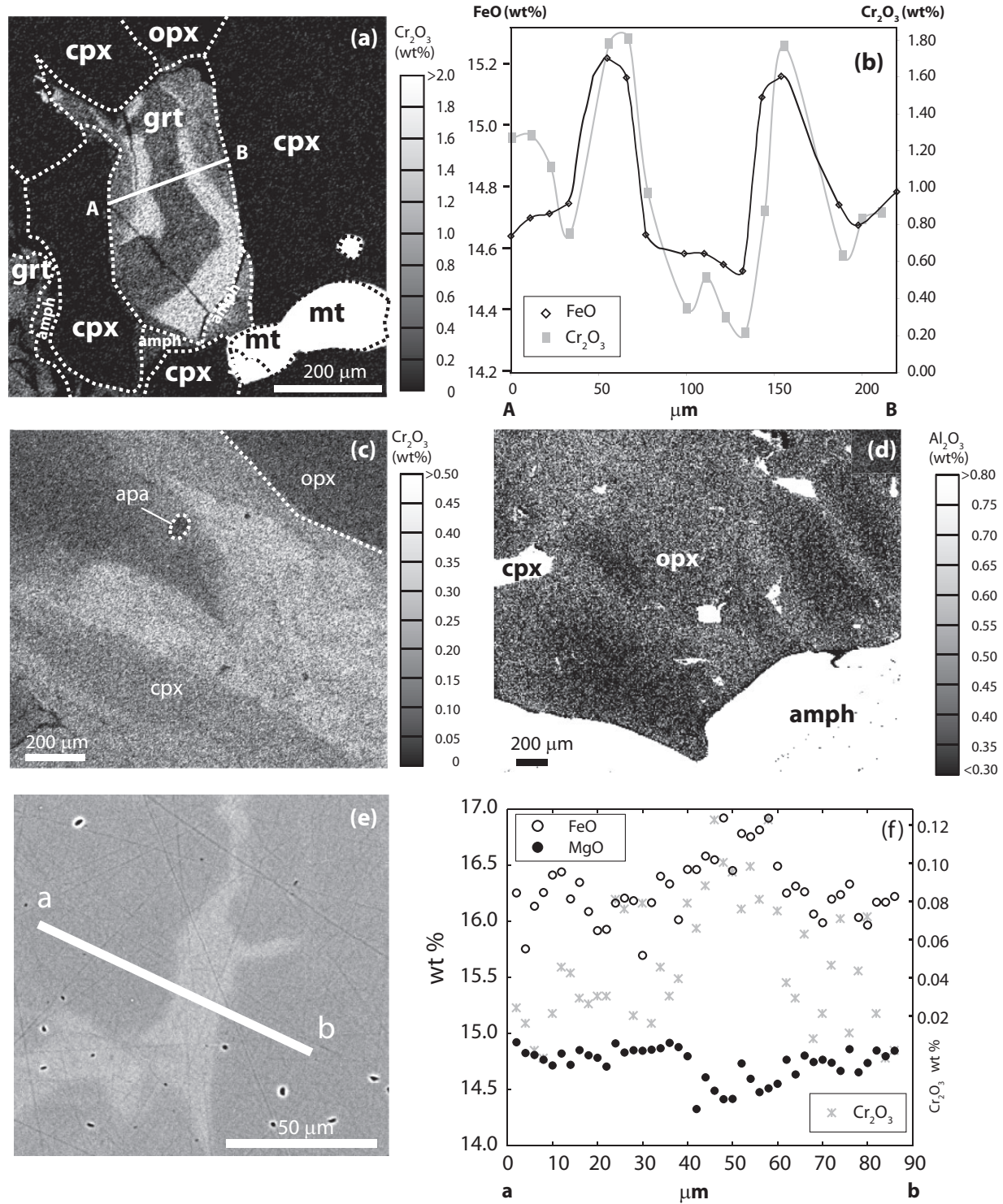


Fig. 11. (a) Compositional map of Cr_2O_3 (lighter shades) showing the 'veining' pattern of garnet in the most pristine peridotite samples (zone 1a, gp). In other examples (not shown here) the 'veining' is more irregular or patchy. The line from A to B corresponds to the profile shown in (b) for FeO and Cr_2O_3 analyses measured by EMP; the sharp compositional contrasts should be noted. (c) Compositional map of Cr_2O_3 in clinopyroxene of phlogopite-garnet-websterite (zone 5a, pgw) showing complex 'veining' patterns of Cr_2O_3 in clinopyroxene. (d) Compositional map of Al_2O_3 in orthopyroxene in coarse-grained phlogopite-garnet-websterite (zone 4, cpw) showing higher Al_2O_3 domains surrounding darker low Al_2O_3 content cores. (e) Back-scattered electron image of 'veining' in garnet from garnetite (zone 6). The compositional contrast is caused by variations in Fe, Mg and Cr content. (f) Compositional profiles of Fe, Mg and Cr along the transect indicated in (e).

Table 4: Whole-rock Rb–Sr isotope data

Sample	Rb (ppm)	Sr (ppm)	Rb/Sr	$^{87}\text{Sr}/^{86}\text{Sr}$	$^{87}\text{Rb}/^{86}\text{Sr}$	$^{87}\text{Sr}/^{86}\text{Sr}_i$ (397.2 Ma)	$^{87}\text{Sr}/^{86}\text{Sr}_i$ (366.1 Ma)
<i>Zone 1c (ow)</i>							
SV06-P1	1.85	48.11	0.038	0.723753 ± 7	0.111	0.723123	0.723172
SV06-P2	0.57	48.32	0.012	0.722805 ± 9	0.034	0.722612	0.722627
<i>Zone 2 (gw)</i>							
SV06-P3	15.13	40.19	0.376	0.741268 ± 35	1.093	0.735087	0.735572
<i>Zone 4 (cpgw)</i>							
SV06-P6	64.2	73.44	0.874	0.749024 ± 5	2.539	0.734660	0.735788
SV06-P7	39.09	79.37	0.493	0.742325 ± 6	1.430	0.734238	0.734873
<i>Zone 6 (ig, g)</i>							
SV06-P8	204.53	13.74	14.886	0.965216 ± 12	44.152	0.715485	0.735089
<i>Zone 7c (ro)</i>							
SV06-D1	1.18	61.13	0.019	0.737585 ± 8	0.056	0.737268	0.737293
<i>Leucosomes</i>							
SV06-G1	53.42	89.41	0.597	0.747837 ± 6	1.735	0.738021	0.738792
SV06-G3	99.6	93.72	1.063	0.791692 ± 19	3.100	0.774158	0.775534
SV06-G5	143.44	202.3	0.709	0.758210 ± 10	2.062	0.746549	0.747465
<i>Gneiss</i>							
SV06-G2	147.42	122.04	1.208	0.766300 ± 13	3.515	0.746419	0.747980
SV06-G4	130.94	198.97	0.658	0.744274 ± 8	1.911	0.733466	0.734314
SV06-G6	131.9	142.64	0.925	0.763004 ± 9	2.690	0.747790	0.748984
<i>Secondary veins (cutting gw and cpgw respectively)</i>							
SV06-P4	8.63	32.42	0.266	0.738614 ± 6	0.772	0.734245	0.734588
SV06-P5	48.73	75.08	0.649	0.745332 ± 9	1.885	0.734672	0.735508

Rb and Sr concentrations are determined by XRF. All errors are 2σ . Errors in $^{87}\text{Rb}/^{86}\text{Sr}$ isotope ratios are 1%.

g). Chrome contents in peridotite clinopyroxene (zone 1a, gp) are low and vary from 0.04 to 0.26 wt % without variations within single minerals. In contrast, Cr_2O_3 in clinopyroxene from websterite (zone 5a, pgw) varies from 0.04 to 0.95 wt % and from 0.13 to 0.49 wt % in single minerals that have complex compositional veining (Fig. 11c). No Cr was detected in clinopyroxene in retro-omphacite (zone 7c, ro). In orthopyroxene, Al_2O_3 is the oxide that shows most variation, usually in typical bowl-shaped patterns as documented by Vrijmoed *et al.* (2006). However, as shown in Fig. 11, the distribution of Al_2O_3 is more complex for the large orthopyroxene grains of the coarse-grained phlogopite–garnet–websterites (zone 4, cpgw).

Isotope geochemistry

Rb–Sr isotope systematics

Rubidium–Sr isotope data for selected samples from peridotite (zone 1a, gp), websterite (zone 1c, ow; zone 4, cpgw), garnetite (zone 6, ig and g), gneiss and leucosomes within gneiss are presented in Table 4. Initial $^{87}\text{Sr}/^{86}\text{Sr}$ ratios (calculated at 397 Ma, based on the zircon age

determined for garnetite) are plotted in Fig. 12, together with data for the nearby Molde augengneiss, Hustad Complex and eclogites in gneiss in the area of the Svartberget body for comparison. In the field, the late-stage alteration (our secondary veins) is easily distinguished from the primary UHP veins. Samples SV06-P4 and SV06-P5 (zones 2 and 4; gw and cpgw, respectively), clearly affected by secondary alteration, show that this late-stage alteration did not have any noticeable effect on the Sr isotope system (Table 4 and Fig. 12).

It is immediately evident that all the Svartberget units, including minerals that define the high-pressure assemblage (clinopyroxene and garnet), are much more radiogenic than expected mantle values at 397 Ma. The lowest $^{87}\text{Sr}/^{86}\text{Sr}_i$ of 0.714 was found in the garnetite (zone 6, ig and g), with the two olivine–websterite samples of zone 1c (ow) being ~ 0.723 . The majority of samples are significantly more radiogenic, with $^{87}\text{Sr}/^{86}\text{Sr}_i$ ratios of ~ 0.735 for peridotite (zone 1a, gp), websterite (zone 4, cpgw; zone 5a, pgw), retrograde omphacite (zone 7c, ro), and the least evolved gneiss and leucosome compositions. The

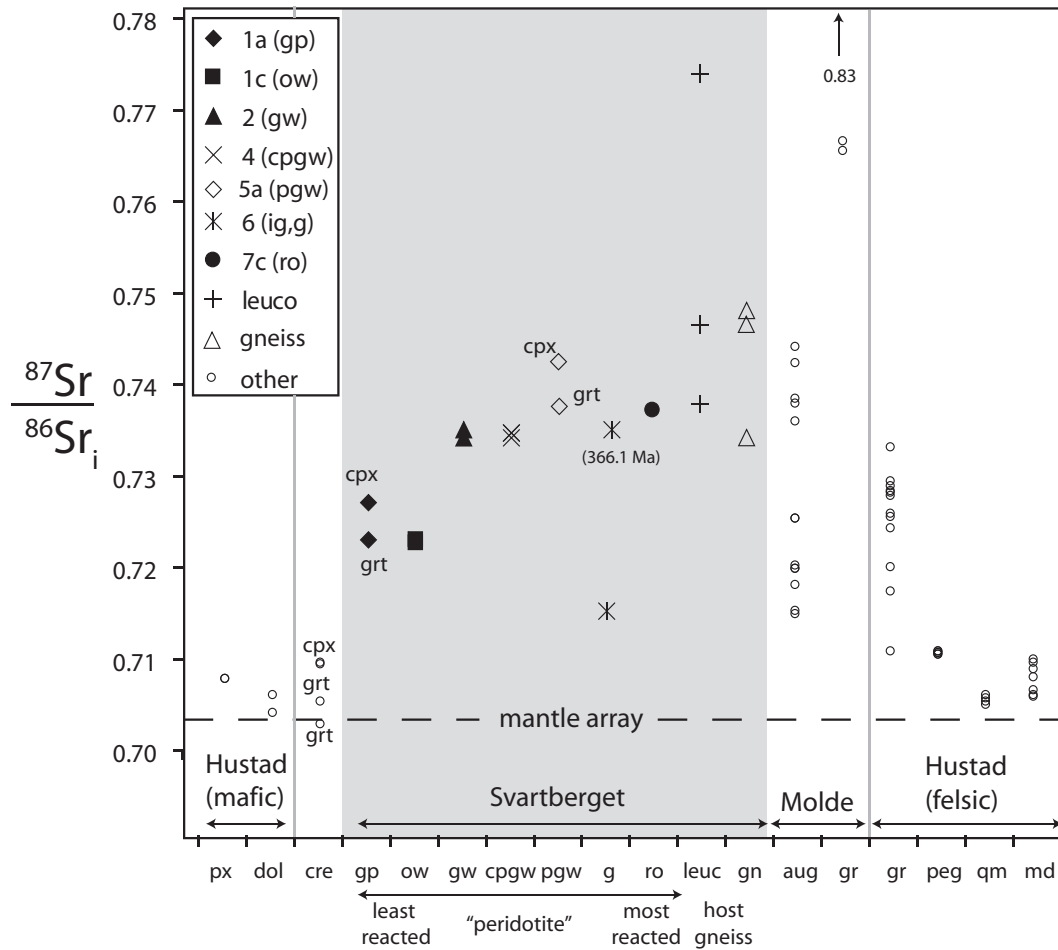


Fig. 12. Initial $^{87}\text{Sr}/^{86}\text{Sr}_i$ ratios calculated at 397 Ma (zircon age in garnetite, Fig. 13) plotted for each zone along with Sr isotope data for similar rock types in the region. The zones along the x-axis are organized from least to most metasomatized, preceded by mafic (or ultramafic) rocks of the Hustad complex (Austrheim *et al.*, 2003) and two country-rock eclogites [samples 79 and 99 of Vrijmoed *et al.* (2006)]. To the right are data for felsic rock types of the Molde area (Harvey, 1983) and the Hustad igneous complex. Abbreviations: px, pyroxenite; dol, dolerite; cre, country rock eclogite; gp, garnet-peridotite; ow, olivine-websterite; gw, garnet-websterite; cpgw, coarse phlogopite-garnet-websterite; pgw, phlogopite-garnet-websterite; g, garnetite; ro, retro-omphacitite; leuc, leucosome; gn, gneiss; aug, augengneiss; gr, granite; peg, pegmatite; qm, quartz monzonite; md, monzodiorite.

other leucosomes and gneiss yield higher $^{87}\text{Sr}/^{86}\text{Sr}_i$ up to 0.78. It is remarkable that the latter are much more radiogenic than the granitic and pegmatitic components of the Hustad complex (Austrheim *et al.*, 2003), but comparable with the more radiogenic compositions of augengneiss and granite from Molde (Harvey, 1983). The shift of the Svartberget peridotite and websterite to more radiogenic Sr isotope compositions is consistent with metasomatic addition of radiogenic Sr from the country rock.

Geochronology

To determine the timing of the partial melting that led to the leucosome formation in the gneiss, we separated zircons and monazites from one of these leucosomes (sample SV07-8, taken from the same leucosome as SV06-G5). Furthermore, to constrain when the garnetite veins

formed, we separated zircon and rutile from a garnetite (zone 6b, sample SV06-1A), along with zircons from the amphibole-pegmatite core in the middle of a retro-omphacitite zone (zone 8, sample SV07-1).

Garnetite (zone 6b, SV06-1A). All zircons separated from the garnetite sample were anhedral, transparent, colourless, homogeneous, rounded grains without inclusions. Three single zircon grains, two large and one small, and a group of four small grains were measured (Table 5). Uranium contents in the zircons are relatively high and vary from 173 to 830 ppm, and the Th/U ratio ranges between 0.024 and 0.056. The analyses are variously discordant and fit on two distinct lines through the least discordant data point, yielding a lower intercept age of 397.2 ± 1.2 Ma and upper intercept ages of about 1622 Ma and 1759 Ma (Fig. 13). This divergence indicates either

Table 5: U–Pb isotopic TIMS mineral data for leucosome in host rock gneiss, garnetite (zone 6b, g) and pegmatite core (zone 8) in garnetite of the Svartberget peridotite body

Sample	U (ppm)	Th/U	Pb _c (pg)	²⁰⁶ Pb/ ²⁰⁴ Pb	²⁰⁷ Pb/ ²³⁵ U	²⁰⁶ Pb/ ²³⁸ U	rho	²⁰⁷ Pb/ ²⁰⁶ Pb	²⁰⁶ Pb/ ²³⁸ U	²⁰⁷ Pb/ ²³⁵ U	²⁰⁷ Pb/ ²⁰⁶ Pb	Disc (%)
<i>Leucosome (SV07-8)</i>												
Z[1],an,cl,l,(1)	n.d.	n.d.	1.1	2482	n.d.	n.d.	n.d.	0.09668 ± 38	n.d.	—	1561.1 ± 7.3	—
Z[1],eu,br,sm,(1)	4300	0.043	1.4	13028	0.5209 ± 14	0.06708 ± 16	0.93	0.05632 ± 6	418.5 ± 1.0	425.7 ± 0.9	465.0 ± 2.2	10
Z[1],an,br,l,(10)	3000	0.004	2.6	45820	0.4744 ± 11	0.06296 ± 13	0.96	0.05465 ± 4	393.6 ± 0.8	394.2 ± 0.8	397.8 ± 1.5	1.1
Z[1],an,cl,l,(3)	10200	0.010	2.8	43824	0.4734 ± 13	0.06284 ± 16	0.97	0.05464 ± 4	392.9 ± 0.9	393.5 ± 0.9	397.3 ± 1.5	1.2
Z[1],eu,br,l,(1)	30000	0.011	2.2	43455	0.3915 ± 14	0.05189 ± 17	0.98	0.05471 ± 4	326.1 ± 1.0	335.4 ± 1.0	400.6 ± 1.7	19
Z[1],eu,br (1)	7800	0.005	2.7	11628	0.4738 ± 12	0.06293 ± 13	0.94	0.05461 ± 5	393.4 ± 0.8	393.8 ± 0.8	396.3 ± 1.9	0.8
Z[1],eu,br (3)	2600	0.005	1.6	18956	0.4759 ± 13	0.06308 ± 14	0.94	0.05473 ± 5	394.3 ± 0.9	395.3 ± 0.9	401.1 ± 2.1	1.7
M[1],an,cl (1)	6800	15.94	7.3	3632	0.4641 ± 13	0.06226 ± 13	0.86	0.05407 ± 8	389.4 ± 0.8	387.1 ± 0.9	373.8 ± 3.2	-4.3
M[1],an,cl (11)	1200	11.80	14.6	3408	0.4630 ± 12	0.06195 ± 12	0.89	0.05421 ± 6	387.5 ± 0.8	386.3 ± 0.8	379.7 ± 2.6	-2.1
M[1],an,py,l,(18)	380	12.80	12	2244	0.4594 ± 15	0.06127 ± 18	0.78	0.05438 ± 12	383.4 ± 1.1	383.8 ± 1.1	386.8 ± 4.8	0.9
M[1],an,py,sm,(12)	280	15.80	16	842	0.4676 ± 25	0.06262 ± 21	0.66	0.05416 ± 22	391.6 ± 1.3	389.6 ± 1.7	377.7 ± 8.9	-3.8
<i>Garnetite (g) (SV06-1A)</i>												
Z[4],an,cl,sm,(24)	270	0.052	6.6	4193	0.5660 ± 14	0.06880 ± 14	0.90	0.05967 ± 6	428.9 ± 0.8	455.4 ± 0.9	591.5 ± 2.3	28
Z[1],an,cl,l,(10)	170	0.056	1.7	4410	0.5922 ± 17	0.07085 ± 18	0.79	0.06062 ± 11	441.3 ± 1.1	472.3 ± 1.1	625.8 ± 3.9	30
Z[1],an,cl,sm,(3)	830	0.047	1.0	10791	0.5210 ± 27	0.06591 ± 34	0.90	0.05734 ± 14	411.5 ± 2.1	425.9 ± 1.8	504.5 ± 5.2	19
Z[1],an,cl,l,(15)	250	0.024	1.6	9578	0.4815 ± 12	0.06374 ± 15	0.86	0.05479 ± 7	398.3 ± 0.9	399.1 ± 0.8	403.8 ± 2.9	1.4
R[7],fr,r,l,(406)	190	0.001	23	12776	0.4606 ± 12	0.06139 ± 14	0.95	0.05442 ± 5	384.0 ± 0.9	384.7 ± 0.9	388.4 ± 1.9	1.2
R[7],fr,r,l,(406)	190	0.001	23	12807	0.4606 ± 11	0.06139 ± 13	0.96	0.05442 ± 4	384.1 ± 0.8	384.7 ± 0.8	388.3 ± 1.6	1.1
<i>Pegmatite core (peg) (SV07-1)</i>												
Z[1],eu,br,l,(1)	36000	0.077	8.4	16401	0.4594 ± 16	0.06119 ± 20	0.97	0.05445 ± 5	382.8 ± 1.2	383.8 ± 1.1	389.7 ± 1.9	1.8
Z[1],eu,br,sm,(1)	6900	0.091	1.1	24708	0.4648 ± 14	0.06190 ± 18	0.95	0.05446 ± 5	387.1 ± 1.1	387.6 ± 1.0	390.3 ± 2.1	0.8
Z[1],an,br,l,(10)	14300	0.062	10	54354	0.4634 ± 17	0.06172 ± 22	0.98	0.05446 ± 4	386.1 ± 1.3	386.6 ± 1.2	389.9 ± 1.5	1.0
Z[1],an,br,sm,(5)	8900	0.067	2.2	76426	0.4640 ± 12	0.06179 ± 14	0.96	0.05447 ± 4	386.5 ± 0.9	387.0 ± 0.8	390.4 ± 1.6	1.0

Errors are 2σ (abs). Pb_c, common lead; Disc., discordance; Z, zircon; M, monazite; R, rutile; eu, euhedral; an, anhedral; sub, subhedral; br, brown; cl, colourless; py, pale yellow; r, red; sm, small; l, large; fr, fragment; [n], number of grains; (n), weight in U concentrations are known to better than 10%, except those near the 1 μ g resolution of the balance.

inheritance of multiple age components or the effects of post-Caledonian Pb loss that displaced some of the data below an original mixing line. The rutile separates consisted of deep red, transparent, anhedral, angular fragments. A fraction of seven large grains, aliquoted after dissolution and measured in duplicate (Table 5), gives a mean ²⁰⁷Pb/²⁰⁶Pb age of 388.3 ± 1.2 Ma.

Leucosome (SV07-8). The zircon population in the leucosome ranges from euhedral, light brown, prismatic crystals to dark brown and colourless, anhedral angular grains. Euhedral crystals commonly have dark brown rounded cores with a light brown to colourless euhedral rim. Four euhedral grains that showed no core and three anhedral transparent grains, two of which were colourless and one brown, were picked for analysis. Their U content is very high, varying from 2500 to 30000 ppm, with no simple relationship between colour and U concentration. The Th/U ratios are low at 0.004–0.043 (Table 5).

Four zircon analyses are clustered close to the concordia curve and are collinear with a more discordant one, defining a lower intercept age of 391.2 ± 0.8 Ma and an upper intercept of 962 ± 34 Ma (Fig. 13). The latter reflects the presence of a Sveconorwegian xenocrystic component. Another clear grain, however, yielded an older ²⁰⁷Pb/²⁰⁶Pb age of 1561 Ma (but no U–Pb age), indicative of a heterogeneous inheritance. The lower intercept age of 391.2 ± 0.8 Ma is taken to date the time of formation of the leucosome. The sixth analysis, of a brown zircon containing 3% U, is much more discordant and was probably affected by Pb loss.

Coexisting monazite occurs as a morphologically uniform population of colourless to pale yellow transparent anhedral grains. Four yellow grains of different size were analysed. Their U content varies considerably from 280 to 6800 ppm and Th/U is 11.8–16.2. Three analyses are reversely discordant, presumably owing to an excess in initial

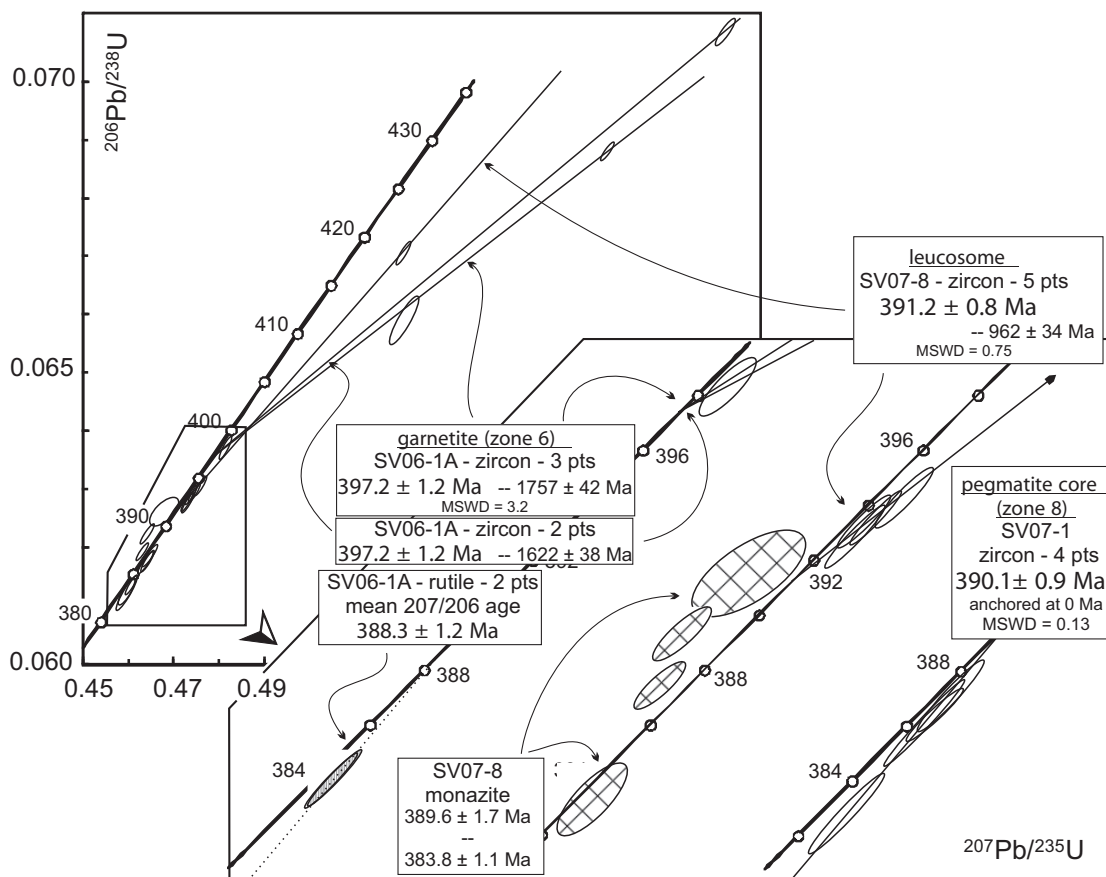


Fig. 13. Concordia diagrams showing U–Pb data for the Svartberget rocks. Ellipses indicate the 2σ error. (See text for discussion.)

^{230}Th (Schärer, 1984), and are scattered, the oldest one yielding a $^{207}\text{Pb}/^{235}\text{U}$ age of 389.6 ± 1.7 Ma. A fourth analysis is concordant, but younger at 383.8 ± 1.1 Ma (Fig. 13).

Pegmatitic core (zone 8, SV07-1). The sampled amphibole-pegmatite that occurs in the core of some veins of the Svartberget peridotite contains a very similar population of zircons to that extracted from leucosome sample SV07-8. Two large and two small sub-millimetre-sized transparent brown grains, euhedral and anhedral respectively, that appeared homogeneous under the microscope were picked for analysis (Table 5). Uranium content is very high, varying between 6900 and 36 000 ppm; the largest grains have the highest U contents. Th/U ratios are high relative to most of the zircons from the leucosome, varying from 0.062 to 0.091. All four zircon grains are slightly discordant, varying from 0.8 to 1.8%. A discordia line, calculated by anchoring the lower intercept point at 0 Ma, has an upper intercept of 390.1 ± 0.9 Ma (Fig. 13).

DISCUSSION

The lithological, mineralogical, geochemical and radiogenic Sr isotope variation across the zones (1–8) described

above clearly results from the addition of crustally derived material to the Svartberget peridotite, and therefore these rocks are metasomatic in origin. This section discusses the nature and extent of the metasomatic process, the source of the incoming material (the metasomatic agent) and the timing of metasomatism.

The extent of metasomatism and mechanisms involved

Mass-balance calculations

To quantify element transport in and out of the peridotite, mass-balance calculations were performed according to the method of Gresens (1967). Average compositions of the volumetrically largest zones 2 (garnet-websterite, gw), 4 and 5 (coarse-grained phlogopite–garnet-websterite, cpgw; phlogopite- and phlogopite-free garnet-websterite, pgw and pfgw) and 6b (garnetite, g), were compared with the inferred protolith. The total mass loss or gain of each zone was calculated using the area obtained from the digitized geological map (see Table 1). Because of the essentially 2D nature of the outcrop we assumed unit length in the third direction to obtain volume. Errors are

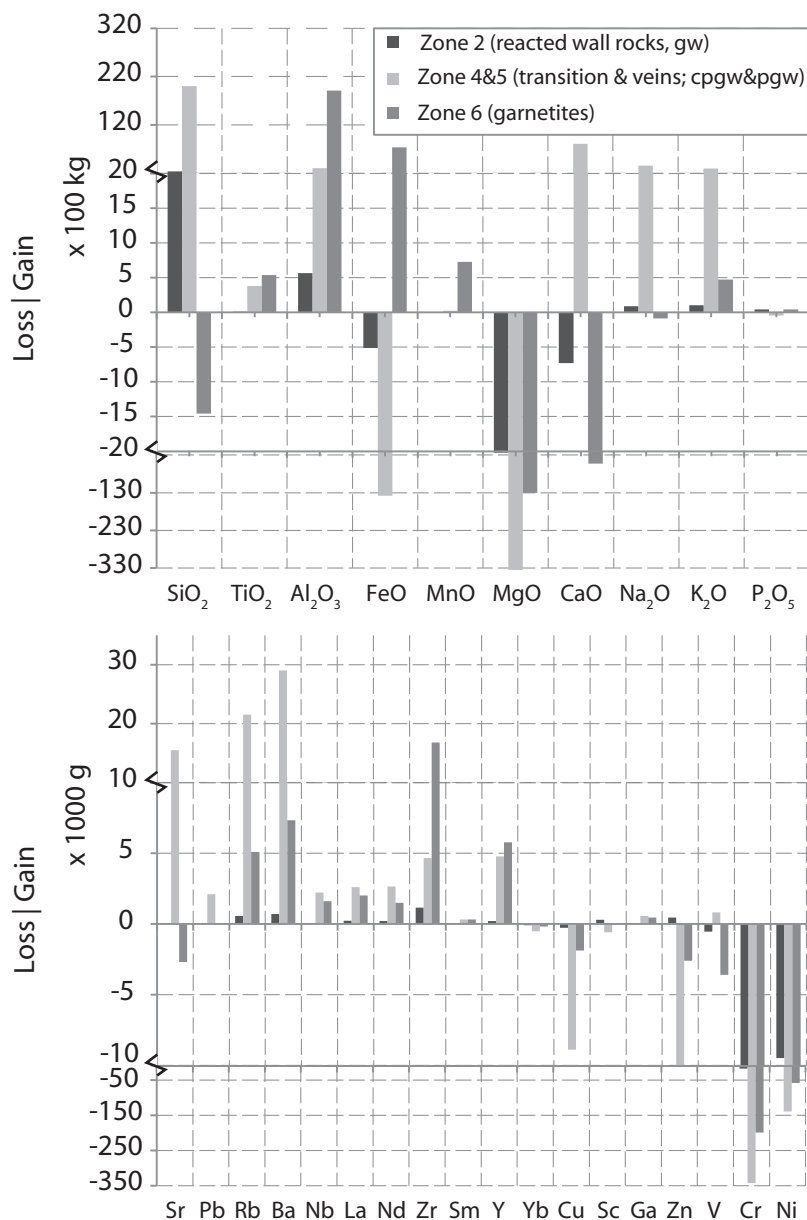


Fig. 14. Mass-balance calculations. The figures indicate the mass difference (gain or loss) of major and trace elements from zones 2, 4, 5 and 6 compared with the wall-rock peridotite (zone 1a, gp).

difficult to assess, but arise from uncertainties in assumed densities, errors in the whole-rock measurements (Suppl. Data Table 1), and errors in the area of the mapped zones. The density for each rock zone was calculated using an Excel spreadsheet from Hacker & Abers (2004) for a pressure of 4.0 GPa and temperature of 800°C. The proportions of mineral endmembers that make up each rock zone were calculated from the mineral composition of the corresponding zone (Table 3) and the estimated mineral modes for each zone are listed under 'Total' in Table 1. The resulting input values for the Excel spreadsheet of Hacker & Abers (2004)

are listed in Suppl. Data Table 7. The used formulae and results of the mass-balance calculations are given in Suppl. Data Table 8. Rock A represents the assumed original rock and B is the metasomatized rock. The calculations assume equal volume replacement [volume factor of unity in equation (10) of Gresens (1967)]. The mass (in kg) of original rock A to be converted is used in equation (10) of Gresens (1967). Applying a volume increase or decrease of 10% does not change the results dramatically.

The results are presented graphically in Fig. 14, which shows the mass gain or loss (in kg) of oxides and trace

elements for the total mapped area (\sim volume) of zones 2, 4, 5 and 6 compared with the wall-rock peridotite (zone 1, gp). These calculations show the oxide or elemental mass that would have been added or removed to produce garnet-websterite (zone 2, gw), coarse-grained phlogopite–garnet-websterite (zone 4 and 5, cpw and pgw, pfgw) and garnetite (zone 6b) from the wall-rock peridotite (zone 1a, gp), assuming that this represents the original compositionally homogeneous rock prior to metasomatism.

Approximately 24×10^3 kg of SiO_2 must be added to about 20 and 153 m^3 of peridotite (zone 1a, gp; Fig. 14) to convert to zone 2 and 4–5 websterites, respectively. Some of this SiO_2 may come from the garnetite where $\sim 1.5 \times 10^3$ kg SiO_2 is in excess, because garnetite has a lower SiO_2 content than peridotite (~ 40 wt % and ~ 48 wt % respectively; see Table 2). However, most SiO_2 ($>95\%$) must be from the external reservoir. Iron has the opposite behaviour because zones 2, 4 and 5 need a combined loss of about 14×10^3 kg Fe_{tot} whereas only about 7×10^3 kg Fe_{tot} is gained by the garnetite. Compared with the peridotite (zone 1a), MgO is lost in all three groups (zones 2, 4, 5 and 6), CaO is lost in zones 2 and 6, but gained in zones 4 and 5, and Al_2O_3 , Na_2O and K_2O are gained, most notably in zones 4 and 5 (cpw; pgw and pfgw). Titanium dioxide and MnO need to be added to the peridotite to a lesser extent. The behaviour of trace elements (lower panel in Fig. 14) is equally variable, with the metasomatized rocks recording net gains and losses. Rubidium and Ba are gained in all metasomatized rocks whereas Sr is gained by websterites (zones 2, 4 and 5), but lost from garnetite. Zirconium and Nb are gained in all metasomatized rocks whereas V, Cu and the refractory elements Cr and Ni are all lost. The light REE (LREE) were gained preferentially over the heavier REE (~ 6.0 kg La and ~ 4.0 kg Nd, compared with ~ 0.7 kg Sm) and Yb records a total of ~ 0.31 kg loss for all three rock groups (zones 2, 4, 5 and 6) compared with the peridotite (zone 1a).

The elements added to the metasomatized rocks (SiO_2 , Al_2O_3 , Rb, Ba, Sr, Zr, Nb, LREE) are all present in high concentrations in the felsic country rocks that host the Svartberget peridotite and the gneiss is therefore the most probable source for the added elements. There are no observational constraints on the destination of elements removed from the peridotite (e.g. Fe_{tot} , MgO, Cr, Ni). We can calculate the effect of adding the same amount of various elements to the gneiss by summing the removed amounts from the assumed precursor peridotite to the mass of the gneiss for a given volume and then renormalizing this amount to the new total mass of the gneiss. If this is done for a band of 10 m width surrounding the peridotite (using the perimeter in Table 1 multiplied by 10 m) a volume of host-rock gneiss of ~ 2500 m^3 is obtained. Using this volume no significant ($<1\%$) major element changes would be predicted. For the trace elements, Cr (and presumably Ni) could significantly increase in the gneiss by

~ 70 ppm (Suppl. Data Table 9). However, as the concentrations in the gneiss before interaction with the peridotite are unknown, it cannot be evaluated whether there was addition of these elements from the peridotite to the gneisses.

Considering the above observations, a scenario is envisaged in which material derived from the country-rock gneiss was the source of the metasomatic addition of elements to the peridotites and the gneisses acted as the host for all elements removed from the peridotite.

Constraints from field data and microtextures

The metasomatic structures of the Svartberget peridotite suggest continuous influx of a metasomatic agent through a network of thin fissures until the end of all mass transport. If sufficient pressure gradients existed these thin fissures may have widened, allowing more material to intrude with time. Such a scenario indicates that the advective component of element transport was mainly focused into a fracture-like porosity whereas the element transport into the unfractured wall-rock predominantly occurred via diffusion (e.g. Norton & Knapp, 1977; Skelton, 2011; John *et al.*, 2013). The ‘immature zones’ are the direct evidence that in certain locations, metasomatism developed through these thin fissures accompanied by a reactive front that progressed perpendicular to the fissures by reactive transport processes. Garnet in the wall-rock peridotite (zone 1) and metasomatized wall-rock (zone 2) is poikilitic and contains inclusions of orthopyroxene, clinopyroxene and olivine. Garnet in zone 6a (inclusion-rich garnetite) also has inclusions of orthopyroxene and clinopyroxene and additionally ilmenite. The complex intra-grain chemical variations indicate that the precursor clinopyroxene and orthopyroxene have been partially transformed to different chemical compositions. Owing to the relatively immobile behaviour of Cr during metamorphic processes, the observed complex distribution of Cr in garnet suggest that a previous Cr-rich phase such as Cr-bearing spinel has been replaced. This suggests that the precursor rock consisted of these minerals and that the metasomatism proceeded by transformation of peridotite to garnetite by means of dissolution–precipitation (Putnis & John, 2010). In contrast, the presence of pre-Caledonian zircons in the veins, which most probably were transported from the host-rock gneiss into the fractures, implies that the fractures were sufficiently wide to allow transport of micrometre-sized solid grains, which is most consistent with the subsequent fracture widening by material influx. This process is also in accordance with the observed eclogites (zone 7) and pegmatites (zone 8), which developed in some cores of the garnetite veins (Figs 3 and 6). Accordingly, when the rock begins to break it starts with a thin fissure along which only small amounts of material can infiltrate. As more material is forced in, the fracture widens and in extreme cases even a felsic, pegmatite-like,

vein may develop (Suppl. Data Fig. 8). Reactions in such a fluid-rich system are efficient and felsic veins in contact with mafic wall-rocks are highly reactive, so that the felsic veins will transform into garnetites by exchanging elements with the wall-rock, which becomes more SiO_2 rich, but MgO and FeO_{tot} poor. This implies that after the injection of such a fluid, element exchange between the felsic vein and peridotite occurs by diffusion in the fluid, whereas the induced dissolution–precipitation processes facilitate reaction front propagation (e.g. Putnis & John, 2010). Fractures that do not fully open and become filled with felsic material are not able to develop into large metasomatic columns owing to the limited supply of reactant material. Hence these fractures remain immature, though reactive, zones.

Interpretation of the ages

The first-order indication of the age data of these metasomatic events is a confirmation that the veining and metasomatism of the Svartberget body occurred during the Caledonian orogeny. The U–Pb data suggest several crystallization events spanning a 10 Myr period. The oldest event is indicated by the crystallization of zircon in the garnetite at 397.2 ± 1.2 Ma, which corresponds to the end of the period determined for UHP metamorphism in the WGR (Root *et al.*, 2004; Kylander-Clark *et al.*, 2009). The garnetite zircon age of 397.2 ± 1.2 Ma overlaps the garnet–clinopyroxene Sm–Nd cooling age of 393.4 ± 3.4 Ma reported for the garnet–peridotite (Vrijmoed *et al.*, 2006). Zircons in the leucosome indicate crystallization at 391.2 ± 0.8 Ma, an age also consistent with the age of the oldest monazite grain in this rock at 389.6 ± 1.7 Ma. This age is also within error of the age of the pegmatitic core (390.1 ± 0.9 Ma) and overlaps the age of formation or recrystallization of rutile in the garnetite at 388.3 ± 1.2 Ma. The four monazite analyses in the leucosome show a spread in age that could be due to either growth of a second generation at or after 383.8 ± 1.1 Ma, the age of the youngest grain analyzed, or to partial resetting. Loss of Pb after formation can expel newly formed and excess Pb, creating a data pattern similar to that observed for the leucosome monazite (Fig. 13; see fig. 9 of Parrish, 1990). Because closure temperatures of Pb in monazite are generally considered to be very high (Cherniak *et al.*, 2004), these age relationships may represent growth, transformation, recrystallization, resorption or alteration. Monazite growth or disturbance at or after 383.8 ± 1.1 Ma, the age of the youngest monazite in the leucosomes, corresponds to the Sm–Nd cooling age of 380.7 ± 5.7 Ma, reported by Vrijmoed *et al.* (2006) for the websterite zones.

From the consistency of these age data we infer that the rocks in the veins within the Svartberget peridotite remained hot (above 650°C) and were affected by fluid activity over an extended period, from ~ 397 Ma until about 380 Ma. This is in accordance with Kylander-Clark *et al.*

(2009). Hence there appear to have been a number of steps: (1) metamorphic growth of zircon in the garnetite with subsequent formation or equilibration of garnet and pyroxene in peridotites at ~ 397 – 393 Ma, which was accompanied by the formation of the metasomatic zones; (2) recrystallization of leucosome and pegmatite cores, and growth or recrystallization of rutile in garnetite at 393–388 Ma owing to late-stage fluid–rock interaction; (3) an additional stage of fluid activity at around 380 Ma. It is also interesting to consider the implications of the Precambrian ages indicated by the inherited zircon grains. The 1622 Ma and possibly older zircon cores in the garnetite can be interpreted either as remnants of older zircons in the peridotite body or as former grains from the gneisses that were transported by the metasomatic agent into the fractures. The 1622 Ma age corresponds to the major period of growth of the crust now making up the WGR (Austrheim *et al.*, 2003). The Pb–Pb age of 1561 Ma for the oldest zircon grain in the leucosome is probably just a minimum age and hence is consistent with a derivation from 1600–1700 Ma crust. The age of 963 ± 34 Ma found in the other zircon from this rock, is consistent with the position at the northern limit of the region influenced by the Sveconorwegian Orogeny (Tucker *et al.*, 1990). Sveconorwegian ages have also been found in the cores of monazites from the area (Terry *et al.*, 2000), but those were interpreted to be in a different tectonostratigraphic unit to the Svartberget body.

Source of the metasomatic agent

Strontium isotope data serve as a useful tracer to constrain the source of the metasomatic agent (Glodny *et al.*, 2003). Figure 12 summarizes the initial whole-rock and mineral $^{87}\text{Sr}/^{86}\text{Sr}$ data for the various zones in the Svartberget peridotite together with regional rock types. The most striking feature of the data is that the Sr isotope compositions of the Svartberget samples lie between those of the garnet–peridotite and those of the leucosomes in the host-rock gneiss. Therefore even the most pristine samples of the wall-rock appear to have been metasomatized to some extent. The Sr from the peridotite is significantly more radiogenic than typical mantle samples at the time of Caledonian orogenesis. Moreover, the Sr isotopic compositions are much more radiogenic than the nearby mafic–ultramafic parts of Hustad Igneous Complex (Austrheim *et al.*, 2003). Svartberget samples are also more radiogenic than peridotites and other ultramafic rocks found elsewhere in the WGR that are interpreted to have been metasomatized by crustal material (Brueckner *et al.*, 2010). The regional gneiss and the leucosomes that host the Svartberget peridotite body have the most radiogenic Sr isotope ratios in this study ($^{87}\text{Sr}/^{86}\text{Sr}$ ratios up to ~ 0.7917). These values are distinctly higher than the granitic components of the Hustad Complex, but similar to those of granite and augen gneiss reported from the Molde region

(Harvey, 1983). The high initial Sr isotope ratios of the gneisses surrounding the Svartberget peridotite are thus not uncommon for such crustal gneisses. The radiogenic Sr isotopic compositions of the leucosomes could furthermore reflect enrichment by eutectic melting involving preferential partial melting of K-feldspar and biotite and hence production of more radiogenic Sr isotope ratios than the typical local basement gneisses (Austrheim *et al.*, 2003).

The initial Sr isotope ratio of the garnetite calculated at 397 Ma is much lower (~ 0.715) than that of the peridotites (0.722–0.734), deviating from the spatial relationship of increasing initial $^{87}\text{Sr}/^{86}\text{Sr}$ towards the veins. The analysed sample contains about 20% phlogopite that reflects the main carrier of the bulk Sr content. The sample has a very high $^{87}\text{Rb}/^{86}\text{Sr}$ ratio (~ 44 ; Table 4) and therefore the initial ratio is very sensitive to the age used in the calculation, with a younger age yielding a considerably higher initial ratio of 0.735 (Table 4). As the closure temperature for the Rb–Sr system in biotite is relatively low (300–400°C), it is likely that the Sr system of the phlogopite remained open longer than that of the other minerals of the various zones in the Svartberget peridotite.

As fluid–rock interaction does not fractionate Sr isotopes (e.g. Baxter & DePaolo, 2000; Glodny *et al.*, 2003) the trend of increasing radiogenic Sr from the most pristine peridotite wall-rock (zone 1a, gp in Fig. 12) to the most reacted parts of the sequence (zone 7c, ro in Fig. 12) seems to reflect mixing of two Sr sources, the peridotite and the surrounding gneiss. In agreement with the mass-balance considerations discussed in the previous section, the leucosomes observed in the gneisses appear to be the probably pristine, now solidified, remnants of the reactive agent that metasomatized the Svartberget peridotite.

Metasomatism of peridotites by surrounding felsic material is a common phenomenon (Malaspina *et al.*, 2009; Brueckner *et al.*, 2010; Scambelluri *et al.*, 2010). In most cases this metasomatism is less pervasive and does not result in the extreme chemical changes observed in the Svartberget peridotite (e.g. Sr isotopes, conversion from peridotite to eclogitic garnetite and omphacite reaching 5–10 cm thicknesses). This is most probably due to the fracture-aided injection of the transitional fluids into a highly stressed peridotite body (Vrijmoed *et al.*, 2009), which generated efficient fluid pathways allowing for advective transport and consequently efficient diffusional element exchange between two connected fluid reservoirs of widely different compositions.

IMPLICATIONS FOR SUBDUCTION ZONE FLUID AND ELEMENT TRANSFER

Aqueous fluids, transitional fluids, or hydrous melts, rich in SiO_2 , LREE and large ion lithophile elements (LILE),

represent possible transport agents that may carry the chemical constituents of a subducting slab into the mantle wedge (Tumiati *et al.*, 2013). Melt generated from this metasomatized mantle wedge may account for the characteristic trace element signature found in magmas above subduction zones (e.g. McCulloch & Gamble, 1991; Manning, 2004; Hermann *et al.*, 2006; Zack & John, 2007). However, the interplay between these agents and the ultramafic rocks of the mantle wedge, and how the slab component finally reaches those parts of the mantle wedge where melting occurs, are not yet fully understood. Felsic gneiss and leucosomes such as those hosting the Svartberget peridotite have comparable chemical compositions (within ~ 1 –2 wt %) to subducted sediments [see comparison in Suppl. Data Fig. 9 with data from Plank & Langmuir (1998)]. The Svartberget peridotite may thus represent an analogue physical-chemical system of the slab–mantle wedge interface. Other workers have also studied similar systems as analogues for the slab–mantle wedge interface to understand some of the processes taking place at depth. Malaspina *et al.* (2006, 2009) showed that the interaction of a felsic fluid or melt with ultramafic rocks at UHP conditions causes significant metasomatism at the interface between the ultramafic bodies and surrounding gneisses, resulting in the formation of metasomatic layers, and to the enrichment of the ultramafic rocks in SiO_2 , LREE, and LILE. As these felsic metasomatic agents are highly reactive, pervasive fluid or melt transport within the mantle wedge seems to be possible only over very small distances. More likely, channelized flow, as observed in dehydrating subducting slabs (e.g. Scambelluri *et al.*, 1997; John & Schenk, 2006; Spandler & Hermann, 2006; John *et al.*, 2008; Beinlich *et al.*, 2010; Spandler *et al.*, 2011), represents the most likely mechanism for longer-distance element transport. It may also be that subducted sedimentary material moves in a diapir-like fashion from the slab into the mantle wedge, thereby carrying most of the required trace elements into the melting region of arc magmatism (Behn *et al.*, 2011; Marschall & Schumacher, 2012). Whereas the field studies of Malaspina *et al.* (2006, 2009) record a system closer to pervasive flow, our study resembles the case of channelized infiltration of a metasomatic agent. Our findings confirm that felsic material is highly reactive in an ultramafic environment and consequently forms metasomatic columns along its flowpaths. These metasomatic columns consist of clinopyroxene-rich, phlogopite-rich, and garnet-rich zones, which owing to their mineral assemblage are well suited to capture most arc signature relevant trace elements (LILE and REE) from the flowing liquid. Fluid-mediated slab-to-wedge material transfer is expected to occur in highly channelized and fast-travelling fluid events (John *et al.*, 2013). However, the intense interaction along the fluid pathways suggests that the metasomatic

agents will be consumed, even though they are released from a large reservoir. This observation has some major implications: long-distance element transport is possible only in conduits or veins that become coated by metasomatic sequences, such as the ones described in this study. This, in turn, requires large, channelized volumes of the slab-derived liquids prior to their injection into the mantle wedge or a continuous reactivation of existing flow structures. It further suggests that the mantle wedge peridotite consumes most of the fluids and melts released by the slab before they may reach regions of arc melt production.

CONCLUSIONS

The garnetite veins, websterite and eclogite zones within the Svartberget peridotite are of metasomatic origin. Mass-balance calculations indicate gains of SiO₂, TiO₂, Al₂O₃, MnO, Na₂O and K₂O by the peridotite, whereas MgO, FeO and CaO are lost during the metasomatism. In addition, Rb, Ba, Sr, Zr, Nb and LREE are added to the peridotite, whereas Zn, V, Cu and the refractory elements Cr and Ni are lost. Based on these data, the felsic Proterozoic gneiss that hosts the peridotite body is considered to have provided the source of the metasomatic agent, which was most probably a hydrous melt-like transitional fluid, generated from the gneiss. The Sr isotope profile perpendicular to the metasomatic zones strongly supports the mixing between the Svartberget peridotite and a transitional fluid that was derived from the surrounding gneisses. The effects of the metasomatic processes result in both major mineralogical and geochemical changes to the peridotite protolith.

Geothermobarometry, Sm–Nd garnet–clinopyroxene isochron ages and single zircon (monazite and rutile) U–Pb TIMS ages from metasomatic zones indicate that metasomatism occurred at the end of the Caledonian UHP metamorphic conditions and during exhumation, but still at very high pressures. Accordingly, the Svartberget peridotite may represent, to date, the best known physical-chemical analogue of how felsic slab-derived material may interact with its surroundings while travelling in a channelized manner within the mantle wedge towards the region of arc magma production.

ACKNOWLEDGEMENTS

We would like to thank Muriel Erambert from the Department of Geosciences at the University of Oslo for assistance and discussion during the microprobe sessions. We further thank Gunborg Bye-Field from the Department of Geosciences at the University of Oslo and Roel van Elsas from the Faculty of Earth and Life Sciences (FALW) at the Vrije Universiteit (VU), Amsterdam, for help with the preparation of whole-rock

powders and mineral separates. Paul Smit from the FALW at the VU in Amsterdam helped with the XRF analyses. We also thank BSc students Marinus den Hartogh, Ineke Wijbrans and supervisor Frank Beunk from the FALW at the VU in Amsterdam for their field- and lab-work contributions (mapping the host rock gneiss and performing some XRF analyses). Reviews by D. Harlov, N. Malaspina, C. Spandler, T. Pettke, Ishimaru and L. Beccaluva significantly improved the paper.

FUNDING

This study was financially supported by the grant of the Norwegian Research Council to PGP, a Centre of Excellence.

SUPPLEMENTARY DATA

Supplementary data for this paper are available at *Journal of Petrology* online.

REFERENCES

- Andersen, T. B. (1998). Extensional tectonics in the caledonides of southern Norway, an overview. *Tectonophysics* **285**, 333–351.
- Austrheim, H., Corfu, F., Bryhni, I. & Andersen, T. B. (2003). The Proterozoic Hustad igneous complex: a low strain enclave with a key to the history of the Western Gneiss Region of Norway. *Precambrian Research* **120**, 149–175.
- Baxter, E. F. & DePaolo, D. J. (2000). Field measurement of slow metamorphic reaction rates at temperatures of 500° to 600°C. *Science* **288**, 1411–1414.
- Beard, B. L., Medaris, L. G., Johnson, C. M., Brueckner, H. K. & Misar, Z. (1992). Petrogenesis of Variscan high-temperature Group A eclogites from the Moldanubian Zone of the Bohemian Massif, Czechoslovakia. *Contributions to Mineralogy and Petrology* **111**, 468–483.
- Becker, H. (1996). Geochemistry of garnet peridotite massifs from lower Austria and the composition of deep lithosphere beneath a Palaeozoic convergent plate margin. *Chemical Geology* **134**, 49–65.
- Behn, M. D., Kelemen, P. B., Hirth, G., Hacker, B. R. & Massonne, H. J. (2011). Diapirs as the source of the sediment signature in arc lavas. *Nature Geoscience* **4**, 641–646.
- Beinlich, A., Klemm, R., John, T. & Gao, J. (2010). Trace-element mobilization during Ca-metasomatism along a major fluid conduit: Eclogitization of blueschist as a consequence of fluid–rock interaction. *Geochimica et Cosmochimica Acta* **74**, 1892–1922.
- Bodinier, J. L. & Godard, M. (2003). Orogenic, ophiolitic, and abyssal peridotites. In: Carlson, R. W. (ed.) *Geochemistry of the Mantle and Core*. Amsterdam: Elsevier, pp. 103–170.
- Bodinier, J. L., Garrido, C. J., Chanefo, I., Bruguier, O. & Gervilla, F. (2008). Origin of pyroxenite–peridotite veined mantle by refertilization reactions: Evidence from the Ronda peridotite (Southern Spain). *Journal of Petrology* **49**, 999–1025.
- Brey, G. P. & Köhler, T. (1990). Geothermobarometry in four-phase lherzolites II. New thermobarometers, and practical assessment of existing thermobarometers. *Journal of Petrology* **31**, 1353–1378.
- Brueckner, H. K. & Medaris, L. G. (2000). A general model for the intrusion and evolution of ‘mantle’ garnet peridotites in high-pressure and ultra-high-pressure metamorphic terranes. *Journal of Metamorphic Geology* **18**, 123–133.

- Brueckner, H. K., Van Roermund, H. L. M. & Pearson, N. J. (2004). An Archean(?) to Paleozoic evolution for a garnet peridotite lens with sub-Baltic Shield affinity within the Seve Nappe Complex of Jamtland, Sweden, central Scandinavian Caledonides. *Journal of Petrology* **45**, 415–437.
- Brueckner, H. K., Carswell, D. A., Griffin, W. L., Medaris, L. G., Van Roermund, H. L. M. & Cuthbert, S. J. (2010). The mantle and crustal evolution of two garnet peridotite suites from the Western Gneiss Region, Norwegian Caledonides: An isotopic investigation. *Lithos* **117**, 1–19.
- Carswell, D. A. (1990). *Eclogite Facies Rocks*. New York: Chapman & Hall.
- Carswell, D. A. & Cuthbert, S. J. (2003). Ultrahigh pressure metamorphism in the Western Gneiss Region of Norway. In: Carswell, D. A. & Compagnoni, R. (eds) *Ultrahigh Pressure Metamorphism*. Budapest: Eotvos University Press, pp. 51–73.
- Carswell, D. A., Harvey, M. A. & Alsamman, A. (1983). The petrogenesis of contrasting Fe–Ti and Mg–Cr garnet peridotite types in the high-grade gneiss complex of Western Norway. *Bulletin de Minéralogie* **106**, 727–750.
- Cherniak, D. J., Watson, E. B., Grove, M. & Harrison, T. M. (2004). Pb diffusion in monazite: A combined RBS/SIMS study. *Geochimica et Cosmochimica Acta* **68**, 829–840.
- Coleman, R. G. & Wang, X. (1995). Overview of the geology and tectonics of UHPM. In: Coleman, R. G. & Wang, X. (eds) *Ultrahigh Pressure Metamorphism (UHPM)*. Cambridge: Cambridge University Press, pp. 1–32.
- Corfu, F. (2004). U–Pb age, setting and tectonic significance of the orthosite–mangerite–charnockite–granite suite, Lofoten–Vesteralen, Norway. *Journal of Petrology* **45**, 1799–1819.
- Droop, G. T. R. (1987). A general equation for estimating Fe³⁺ concentrations in ferromagnesian silicates and oxides from microprobe analyses, using stoichiometric criteria. *Mineralogical Magazine* **51**, 431–435.
- Glodny, J., Austrheim, H., Molina, J. F., Rusin, A. I. & Seward, D. (2003). Rb/Sr record of fluid–rock interaction in eclogites: The Marun-Keu complex, Polar Urals, Russia. *Geochimica et Cosmochimica Acta* **67**, 4353–4371.
- Gresens, R. L. (1967). Composition–volume relationships of metasomatism. *Chemical Geology* **2**, 47–65.
- Hacker, B. R. & Abers, G. A. (2004). Subduction Factory 3: An Excel worksheet and macro for calculating the densities, seismic wave speeds, and H₂O contents of minerals and rocks at pressure and temperature. *Geochemistry, Geophysics, Geosystems* **5**, doi:10.1029/2003GC000614.
- Harvey, M. A. (1983). A geochemical and Rb–Sr study of the Proterozoic augen orthogneisses on the Molde peninsula, west Norway. *Lithos* **16**, 325–338.
- Hermann, J., Spandler, C., Hack, A. & Korsakov, A. V. (2006). Aqueous fluids and hydrous melts in high-pressure and ultra-high pressure rocks: Implications for element transfer in subduction zones. *Lithos* **92**, 399–417.
- Jamtveit, B. (1987). Magmatic and metamorphic controls on chemical variations within the Eiksunddal eclogite complex, Sunnmøre, western Norway. *Lithos* **20**, 369–389.
- John, T. & Schenk, V. (2006). Interrelations between intermediate-depth earthquakes and fluid flow within subducting oceanic plates: Constraints from eclogite facies pseudotachylytes. *Geology* **34**, 557–560.
- John, T., Klemd, R., Gao, J. & Garbe-Schonberg, C. D. (2008). Trace-element mobilization in slabs due to non steady-state fluid–rock interaction: Constraints from an eclogite-facies transport vein in blueschist (Tianshan, China). *Lithos* **103**, 1–24.
- John, T., Gussone, N., Podladchikov, Y. Y., Bebout, G., Dohmen, R., Halama, R., Klemd, R., Magna, T. & Seitz, M. (2012). Volcanic arcs fed by rapid pulsed fluid flow through subducting slabs. *Nature Geoscience* **5**, 489–492.
- Krogh, E. J. & Carswell, D. A. (1995). HP and UHP eclogites and garnet peridotites in the Scandinavian Caledonides. In: Coleman, R. G. & Wang, X. (eds) *Ultrahigh Pressure Metamorphism*. Cambridge: Cambridge University Press, pp. 244–298.
- Krogh, T. E. (1973). A low-contamination method for hydrothermal decomposition of zircon and extraction of U and Pb for isotopic age determinations. *Geochimica et Cosmochimica Acta* **37**, 485–494.
- Kylander-Clark, A. R. C., Hacker, B. R., Johnson, C. M., Beard, B. L. & Mahlen, N. J. (2009). Slow subduction of a thick ultrahigh-pressure terrane. *Tectonics* **28**, doi:10.1029/2007TC002251.
- Labrousse, L., Prouteau, G. & Ganzhorn, A. C. (2011). Continental exhumation triggered by partial melting at ultrahigh pressure. *Geology* **39**, 1171–1174.
- Leake, B. E., Woolley, A. R., Arps, C. E. S., Birch, W. D., Gilbert, M. C., Grice, J. D., Hawthorne, F. C., Kato, A., Kisch, H. J., Krivovichev, V. G., Linthout, K., Laird, J., Mandarino, J. A., Maresch, W. V., Nickel, E. H., Rock, N. M. S., Schumacher, J. C., Smith, D. C., Stephenson, N. C. N., Ungaretti, L., Whittaker, E. J. W. & Guo, Y. Z. (1997). Nomenclature of amphiboles: Report of the subcommittee on amphiboles of the International Mineralogical Association, Commission on New Minerals and Mineral Names. *Canadian Mineralogist* **35**, 219–246.
- Ludwig, K. R. (1999). *Isoplot/Ex version 2.03. A geochronological toolkit for Microsoft Excel*. Berkeley Geochronology Center, Special Publication **1**, 43 p.
- Malaspina, N., Hermann, J., Scambelluri, M. & Compagnoni, R. (2006). Polyphase inclusions in garnet-orthopyroxenite (Dabie Shan, China) as monitors for metasomatism and fluid-related trace element transfer in subduction zone peridotite. *Earth and Planetary Science Letters* **249**, 173–187.
- Malaspina, N., Hermann, J. & Scambelluri, M. (2009). Fluid/mineral interaction in UHP garnet peridotite. *Lithos* **107**, 38–52.
- Manning, C. E. (2004). The chemistry of subduction-zone fluids. *Earth and Planetary Science Letters* **223**, 1–16.
- Marschall, H. R. & Schumacher, J. C. (2012). Arc magmas sourced from mélange diapirs in subduction zones. *Nature Geoscience* **5**, 862–867.
- McCulloch, M. T. & Gamble, J. A. (1991). Geochemical and geodynamical constraints on subduction zone magmatism. *Earth and Planetary Science Letters* **102**, 358–374.
- Medaris, L. G., Beard, B. L., Johnson, C. M., Valley, J. W., Spicuzza, M. J., Jelinek, E. & Misar, Z. (1995). Garnet pyroxenite and eclogite in the Bohemian Massif: geochemical evidence for Variscan recycling of subducted lithosphere. *Geologische Rundschau* **84**, 489–505.
- Mork, M. B. E. (1985). A gabbro to eclogite transition on Flemsøy, Sunnmøre, Western Norway. *Chemical Geology* **50**, 283–310.
- Norton, D. & Knapp, R. (1977). Transport phenomena in hydrothermal systems—nature of porosity. *American Journal of Science* **277**, 913–936.
- O'Neill, H. S. C. (1980). An experimental study of Fe–Mg partitioning between garnet and olivine and its calibration as a geothermometer: corrections. *Contributions to Mineralogy and Petrology* **72**, 337–337.
- O'Neill, H. S. C. & Wood, B. J. (1979). An experimental study of Fe–Mg partitioning between garnet and olivine and its calibration as a geothermometer. *Contributions to Mineralogy and Petrology* **70**, 59–70.
- Parrish, R. R. (1990). U–Pb dating of monazite and its applications to geological problems. *Canadian Journal of Earth Sciences* **27**, 1431–1450.

- Pearce, J. A. (1983). Role of the sub-continental lithosphere in magma genesis at active continental margins. In: Hawkesworth, C. J. & Norry, M. J. (eds) *Continental Basalts and Mantle Xenoliths*. Nantwich: Shiva, pp. 230–249.
- Plank, T. & Langmuir, C. H. (1998). The chemical composition of subducting sediment and its consequences for the crust and mantle. *Chemical Geology* **145**, 325–394.
- Powell, R. (1985). Regression diagnostics and robust regression in geothermometer/geobarometer calibration: the garnet–clinopyroxene geothermometer revisited. *Journal of Metamorphic Geology* **3**, 231–243.
- Pouchou, J. L. & Pichoir, F. (1984). Quantitative microanalytic possibilities using a new formulation of matrix effects. *Journal de Physique* **45**, 17–20.
- Putnis, A. & John, T. (2010). Replacement processes in the Earth's crust. *Elements* **6**, 159–164.
- Rampone, E. & Morten, L. (2001). Records of crustal metasomatism in the garnet peridotites of the Ulten Zone (Upper Austroalpine, Eastern Alps). *Journal of Petrology* **42**, 207–219.
- Reverdatto, V. V., Selyatitskiy, A. Y. & Carswell, D. A. (2008). Geochemical distinctions between 'crustal' and mantle-derived peridotites/pyroxenites in high/ultrahigh pressure metamorphic complexes. *Russian Geology and Geophysics* **49**, 73–90.
- Root, D. B., Hacker, B. R., Mattinson, J. M. & Wooden, J. L. (2004). Zircon geochronology and ca. 400 Ma exhumation of Norwegian ultrahigh-pressure rocks: an ion microprobe and chemical abrasion study. *Earth and Planetary Science Letters* **228**, 325–341.
- Scambelluri, M., Pettker, T. & van Roermund, H. L. M. (2008). Majoritic garnets monitor deep subduction fluid flow and mantle dynamics. *Geology* **36**, 59–62.
- Scambelluri, M., van Roermund, H. L. M. & Pettker, T. (2010). Mantle wedge peridotites: Fossil reservoirs of deep subduction zone processes: Inferences from high and ultrahigh-pressure rocks from Bardane (Western Norway) and Ulten (Italian Alps). *Lithos* **120**, 186–201.
- Scambelluri, M., Piccardo, G. B., Philippot, P., Robbiano, A. & Negretti, L. (1997). High salinity fluid inclusions formed from recycled seawater in deeply subducted alpine serpentinite. *Earth and Planetary Science Letters* **148**, 485–499.
- Schärer, U. (1984). The effect of initial ^{230}Th disequilibrium on young U–Pb ages: the Makalu case, Himalaya. *Earth and Planetary Science Letters* **67**, 191–204.
- Sekine, T. & Wyllie, P. J. (1982). Phase relationships in the system $\text{KAlSi}_3\text{O}_8\text{--Mg}_2\text{SiO}_4\text{--SiO}_2\text{--H}_2\text{O}$ as a model for hybridization between hydrous siliceous melts and peridotite. *Contributions to Mineralogy and Petrology* **79**, 368–374.
- Skelton, A. (2011). Flux rates for water and carbon during greenschist facies metamorphism. *Geology* **39**, 43–46.
- Spandler, C. & Hermann, J. (2006). High-pressure veins in eclogite from New Caledonia and their significance for fluid migration in subduction zones. *Lithos* **89**, 135–153.
- Spandler, C., Pettker, T. & Rubatto, D. (2011). Internal and external fluid sources for eclogite-facies veins in the Monviso meta-ophiolite, Western Alps: implications for fluid flow in subduction zones. *Journal of Petrology* **52**, 1207–1236.
- Spengler, D., van Roermund, H. L. M., Drury, M. R., Ottolini, L., Mason, P. R. D. & Davies, G. R. (2006). Deep origin and hot melting of an Archaean orogenic peridotite massif in Norway. *Nature* **440**, 913–917.
- Stacey, J. S. & Kramers, J. D. (1975). Approximation of terrestrial lead isotope evolution by a two-stage model. *Earth and Planetary Science Letters* **26**, 207–221.
- Sun, S. S. & McDonough, W. F. (1989). Chemical and isotopic systematics of oceanic basalts: implications for mantle composition and processes. In: Saunders, A. D. & Norry, M. J. (eds) *Magmatism in the Ocean Basins*. Geological Society, London, Special Publications **42**, 313–345.
- Terry, M. P., Robinson, P., Ravna, E. J. K., Hamilton, M. A. & Jercinovic, M. J. (2000). Monazite geochronology of UHP and HP metamorphism, deformation, and exhumation, Nordøyane, Western Gneiss Region, Norway. *American Mineralogist* **85**, 1651–1664.
- Torsvik, T. H., Smethurst, M. A., Meert, J. G., VanderVoo, R., McKerrow, W. S., Brasier, M. D., Sturt, B. A. & Walderhaug, H. J. (1996). Continental break-up and collision in the Neoproterozoic and Palaeozoic—A tale of Baltica and Laurentia. *Earth-Science Reviews* **40**, 229–258.
- Tucker, R. D., Krogh, T. E. & Råheim, A. (1990). Proterozoic evolution and age-province boundaries in the central part of the Western Gneiss Region, Norway; results of U–Pb dating of accessory minerals from Trondheimsfjord to Geiranger. In: Gower, C. F., Rivers, T. & Ryan, B. (eds), *Mid-Proterozoic Laurentia-Baltica*, Geological Association of Canada, Special Papers **38**, 149–173.
- Tumiati, S., Fumagalli, P., Tiraboschi, C. & Poli, S. (2013). An experimental study on COH-bearing peridotite up to 3.2 GPa and implications for crust–mantle recycling. *Journal of Petrology* **54**, 453–479.
- Vrijmoed, J. C., Smith, D. C. & van Roermund, H. L. M. (2008). Raman confirmation of microdiamond in the Svartberget Fe–Ti type garnet peridotite, Western Gneiss Region, Western Norway. *Terra Nova* **20**, 295–301.
- Vrijmoed, J. C., Van Roermund, H. L. M. & Davies, G. R. (2006). Evidence for diamond-grade ultra-high pressure metamorphism and fluid interaction in the Svartberget Fe–Ti garnet peridotite–websterite body, Western Gneiss Region, Norway. *Mineralogy and Petrology* **88**, 381–405.
- Vrijmoed, J. C., Podladchikov, Y. Y., Andersen, T. B. & Hartz, E. H. (2009). An alternative model for ultra-high pressure in the Svartberget Fe–Ti garnet-peridotite, Western Gneiss Region, Norway. *European Journal of Mineralogy* **21**, 1119–1133.
- Zack, T. & John, T. (2007). An evaluation of reactive fluid flow and trace element mobility in subducting slabs. *Chemical Geology* **239**, 199–216.